OPEN ACCESS
Journal of Multidisciplinary Applied Natural Science Vol. 5 No. 2 (2025) https://doi.org/10.47352/jmans.2774-3047.258
Check for updates
Research Article

Investigation of New 4-Benzyloxy-2-trichloromethylquinazoline Derivatives as Plasmodium falciparum Dihydrofolate Reductase-thymidylate Synthase Inhibitors: QSAR, ADME, Drug-likeness, Toxicity, Molecular Docking and Molecular Dynamics Simulation

Radite Yogaswara, Harno Dwi Pranowo*, Niko Prasetyo, and Maria Ludya Pulung

Received : December 6, 2024	Revised : March 6, 2025	Accepted : March 10, 2025	Online : May 18, 2025

Abstract
Plasmonium falciparum dihydrofolate reductase-thymidylate synthase (*Pf*DHFR-TS) is one of the most crucial antimalarial targets. Mutations in the binding pocket of this target lead to resistance to the antifolate. The mutations influence the amino acid residues at points 51, 59, 108 and 164 and contribute significantly to malaria not being treated well. Priority should therefore be given to the development of antifolate-resistance drugs. These studies aim to investigate new 4-benzyloxy-2-trichloromethylquinazoline derivatives as *Pf*DHFR-TS inhibitors using QSAR, ADME, drug-likeness, toxicity, molecular docking studies, and molecular dynamics simulations. The best equation model from the QSAR analysis used MLR and PLS statistics to show that the pIC_{50} is linearly related to GATS4e, SpMax AEA(ed), and Mor28e, but inverted when compared to ATS6m and ATSC7m. The predictive ability of the model was confirmed by internal and external validation. In addition, the Y-randomization validation showed that the QSAR model was reliable, robust, and stable, with a cRp^2 score of over 0.5. ADME and drug-likeness predictions confirmed the new QSAR design for molecules S10, S23 and S64. Based on the toxicity results, three molecules are expected to have moderate and non-toxic properties, starting with S23 and then S10 and S64. Molecular docking studies show that all three molecules have high binding energies, 9.869, 9.589, and 9.565 kcal/mol. The amino acid residues Leu46, Asp54, Ser111, and Thr185 play a major role in ligand-receptor interaction in the binding pocket of quadruple mutant *Pf*DHFR-TS. Furthermore, an evaluation of molecular dynamics simulations of three complexes S10-3JSU, S23-3JSU and S64-3JSU demonstrated stable interactions over 100 ns.

Keywords: QSAR, ADME, quinazoline, molecular docking, *Pf*DHFR-TS

1. INTRODUCTION

Protozoa of the genus Plasmodium cause the infectious disease malaria. An infected female Anopheles mosquito bites to spread it. The World Health Organization (WHO) reported 229 million malaria cases globally in 2019, which directly accounted for 409,000 deaths [1][2]. Among *P. falciparum* infections, the degree of the illness and mortality rates are the highest. After the cause of the disease and symptoms were found, many natural and synthetic antimalarial medications were created. First used antimalarial drugs in tropical and subtropical environments are quinolines, naphthoquinones, antifolates, 8-aminoquinolines, and endoperoxides. Multi-drug resistance causes current antimalarial drugs to be less effective. Due to resistance to artemisinin and combination therapies, malaria prophylaxis has declined. Therefore, new antimalarial drugs and drug targets are needed to reduce malaria resistance [3].

An infection caused by this particular species leads to a rapid escalation of parasitemia compared to other species. In addition, their merozoites can infect red blood cells in all individuals. The resistance that this parasite has developed to current malaria therapies is one of the causes of death and leads to treatment failure [2]. Resistance to recommended artemisinin combination therapy (ACT) for malaria treatment has also been reported [4]. Resistance can result from the administration of insufficient doses of drugs or from mutations in several important genes that are linked to the drug targets in the parasite's organism.

*Pf*DHFR-TS is an important target of antimalarial drugs. This class of DHFR inhibitors is ineffective due to mutations that prevent drug binding but retain enzyme activity. The wild type (TM4/8.2), the quadruple drug-resistant mutant

Table 1. Antimalarial activity of 4-benzyloxy-2-trichloromethylquinazoline derivatives [18].

ID	Structure (-R)	IC_{50} (µM)	pIC_{50}	ID	Structure (-R)	IC_{50} (µM)	pIC_{50}
C1*	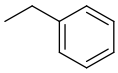	2.0	5.699	C17	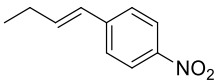	2.6	5.585
C2	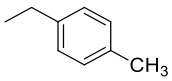	4.0	5.398	C18	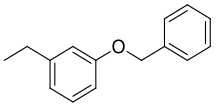	3.8	5.420
C4	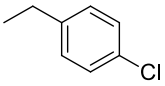	2.5	5.602	C19	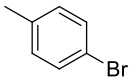	1.8	5.745
C5	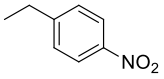	1.8	5.745	C20	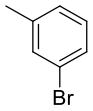	2.3	5.638
C6	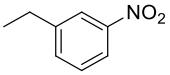	2.2	5.658	C21	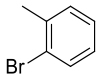	1.9	5.721
C7	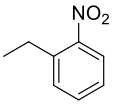	2.3	5.638	C22	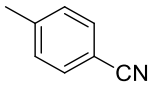	1.6	5.796
C8	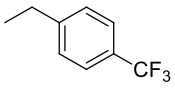	2.8	5.553	C23	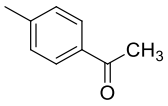	2.3	5.638
C10	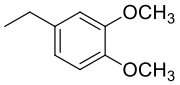	3.9	5.409	C24	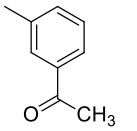	1.7	5.770
C11*	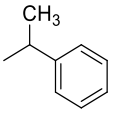	3.3	5.481	C25	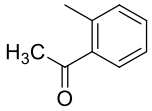	1.5	5.824
C12*	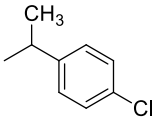	3.5	5.456	C26	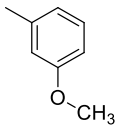	1.9	5.721
C13	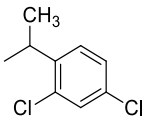	4.2	5.377	C28	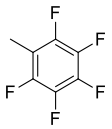	4.4	5.357
C14	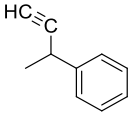	2.4	5.620	C30*	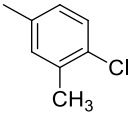	0.9	6.046
C15*	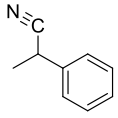	1.5	5.824	C31*	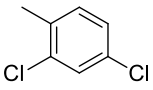	1.2	5.921
C16	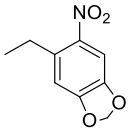	3.1	5.509				

*Test sets

Table 2. Correlation matrix and variation inflation factors of the model descriptors.

Descriptors	ATS6m	ATSC7m	GATS4e	SpMax_AEA(ed)	Mor28e	VIF	MF	p-value
ATS6m	**1.000**					2.41	-0.382	0.0032
ATSC7m	0.153	**1.000**				4.18	-0.375	0.0073
GATS4e	-0.222	0.174	**1.000**			1.43	0.109	0.0001
SpMax_AEA(ed)	0.457	-0.626	-0.405	**1.000**		4.11	1.339	0.0023
Mor28e	-0.204	-0.205	0.446	-0.271	**1.000**	1.91	0.308	0.0001

(V1/S), and the resistant double mutant (K1 CB1) with the antimalarial pyrimethamine (CP6) have crystal structures which show how resistance can be overcome [5][6]. In contrast to CP6, the flexible side chain of WR99210 can bind to the active site and thus improve binding. The single-chain bifunctional *Pf*DHFR-TS dimerizes and organizes itself with a helical insert between the DHFR and TS domains. Positively charged dimer grooves can transport the substrate from the TS to the DHFR active sites. This points to a drug design with antifolate resistance.

Commonly used are sulfadoxine and CP6, which stop the Plasmodium DHFR enzyme. The prevalence of CP6 resistance makes this medication ineffective. CP6 resistance is associated with the DHFR codon 108 Ser-Asn mutation (S108N). Secondary mutations of N51I and C59R increase CP6 resistance, and I164L increases it even more [5]–[9]. In a biochemical test, these mutations produced a notable drop in the sensitivity of the *Pf*DHFR enzyme to CP6 inhibition. Effective in P. falciparum, the antifolate triazine WR99 has quadruple DHFR mutations in S108N, N51I, C59R, and I164L. Low oral bioavailability and gastrointestinal toxicity of WR99210 restrict its in vivo efficacy. To get over these issues, an orally effective prodrug based on WR99210, PS-15 was developed. In vitro and in silico studies of inhibition of *Pf*DHFR-TS activity have examined quinolines [10], triazoles [11][12], sulfonamides [13][14], chalcones [15][16], xanthones [17], and quinazolines [18][19].

Quinazoline is a molecule that is currently being developed as a low molecular weight drug, particularly as an antimalarial drug. The molecule 4 -benzyloxy-2-trichloromethylquinazoline, shown in Fig. S1, was prepared and showed high activity and selectivity for its action against malaria, as previously described [18]. Important for cytotoxicity and antimalarial action are the substituents joined to the benzyloxy group at position 4 [18][20]–[22]. In medicinal chemistry, the quinazoline derivative is a convenient and flexible pharmacophore unit used to generate several bioactive molecules with pharmacological effects including antimalarials, anticancer, antiviral, anti-inflammatory, antimicrobial, cholinesterase inhibitors, antifolate, antitumor, and protein kinase inhibitors [19][20][21]–[28][29]. A computer-aided drug discovery (CADD) approach has to be used to identify a new molecule generated from 4-benzyl-2-trichloromethylquinazoline derivatives against *Pf*DHFR-Ts since the pharmacological effects of the quinazoline structure have become crucial.

CADD is a popular way to study novel molecules versus specific protein targets [30][31]. It was used in addition to *in vitro* and *in vivo* methods in the drug design process. Drug development through trial and error is cumbersome, expensive, and time-consuming. Quantitative structure-activity relationships (QSAR), molecular docking, and ADME studies are among the CADD studies that were able to speed up the filtering of hits to leads and reduce the costs of synthesizing potent drugs [32]–[34]. In this study, QSAR, ADME, drug similarity, toxicity, molecular docking, and molecular dynamics were simulated to pinpoint potential prime candidates for the *in-silico* design of novel *Pf*DHFR-TS inhibitors with improved bioactivity. The QSAR study examines 27 molecules of 4-benzyloxy-2-trichloromethylquinazoline derivatives, which were synthesized by predicting their antimalarial activity based on calculated structural features in numerical values of molecular descriptors [18]. The QSAR models were originally constructed on the basis of multiple linear regression (MLR) and partial least

squares (PLS). The series of 4-benzyloxy-2-trichloromethylquinazoline derivatives was subjected to virtual screening against the quadruple mutant (PDB ID: 3JSU) of the *Pf*DHFR-TS targets. We used the protein targets 3JSU because it was crystal structure of the dihydrofolate reductase-thymidylate synthase (DHFR-TS) of *Plasmodium falciparum*, which is essential for the parasite's metabolism and folic acid synthesis for growth and reproduction [6]. The structural data of the proteins in the Protein Data Bank (PDB) supports molecular modeling and drug ligand binding studies and helps researchers understand the interactions between inhibitors and enzymes. When studying resistance to malaria, researchers can use 3JSU as a mutant target to compare the developed molecules with both the wild type and the mutant forms and thus get a complete picture of their potential against malaria. This approach aimed to identify potential prime candidates by evaluating their docking levels and residual interactions through molecular docking studies. In addition, an evaluation of the properties, drug similarity, and toxicities of ADME was carried out to verify the suitability of the most appropriate inhibitor for potential use as an antimalarial drug.

2. MATERIALS AND METHODS

2.1. Dataset and Biological Activities

The data set used in this study consists of 27 molecules of 4-benzyloxy-2-trichloromethylquinazoline derivatives derived from literature, as shown in Table 1. To avoid data bias in the QSAR studies, activities were set at pIC_{50} (μM) = 6 – log IC_{50} [35]–[37]. The 21 molecules were used as a training set (80%), while the remaining 6 molecules were assigned as a test set (20%). The dataset division of the Drug Theoretical and Cheminformatics Laboratory (DTC Lab) software was used to split the dataset [38].

The minimum size of the dataset is linked to the 5:1 and 10:1 rules, in order to avoid overfitting and generalization. If the data set is very small in relation to the number of features used, the model can learn very specific patterns from the training data, but it cannot be very generalized to the new data set. By applying the 5:1 and 10:1 rules, we reduce the risk of overfitting, as the model has more data to learn from different chemical structure representations. Sufficiently large data sets allow the model to identify and understand more general relationships between the components of the superstructure and their activities. This increases the model's ability to make more accurate predictions about data that is unknown to it. The 5:1 and 10:1 rules help to maintain the reliability and validity of QSAR models by ensuring that the size of the data set is sufficient to produce models that are not only accurate but also capable of being well generalized [39]. The number of descriptors in this study is 5 (n = 5) using the 5:1 rule, 5 × n, i.e. 25 total minimum datasets to be used.

2.2. Structure Optimization and Descriptor Selection

The chemical structures of 27 molecules of 4-benzyloxy-2-trichloromethylquinazoline derivatives were drawn in ChemDraw 12 software and the geometry optimization was calculated in Gaussian 09 software using the DFT method with B3LYP

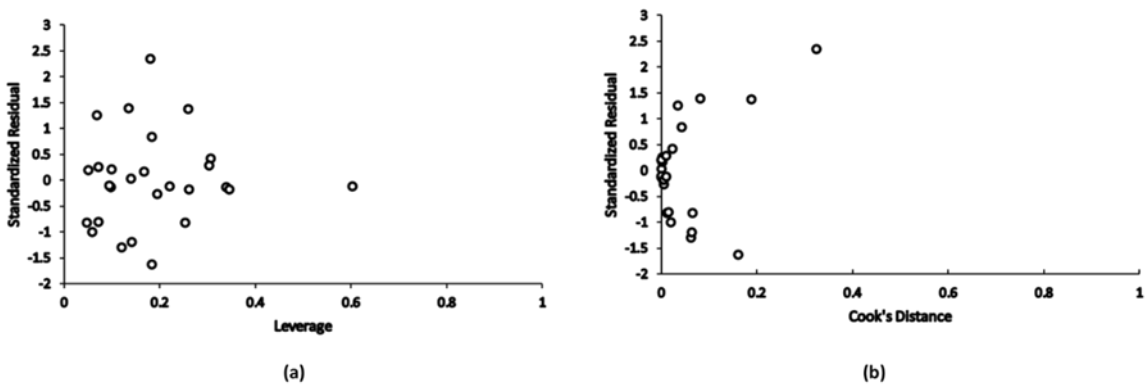

Figure 1. The leverage approach to analyzing the chemical space (outliers). (a) William's diagram, and (b) Cook's Distance.

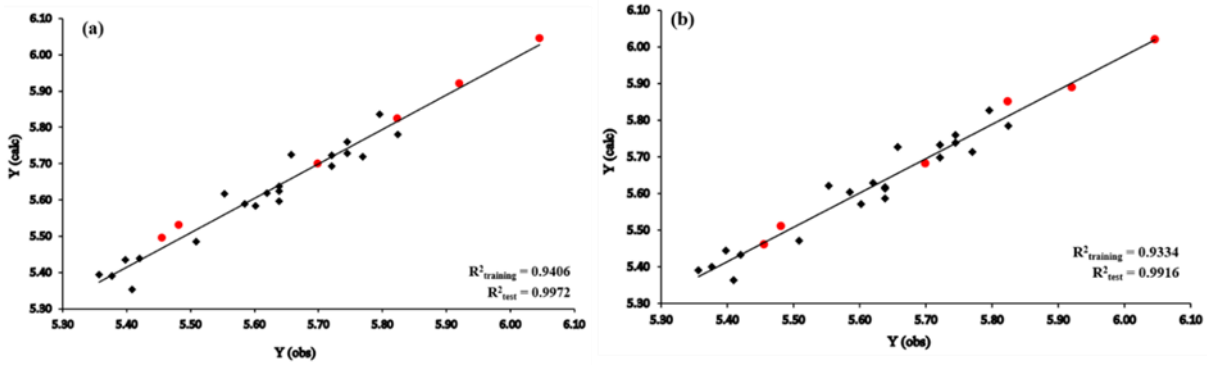

Figure 2. pIC$_{50}$ predicted is Y(calc) vs. pIC$_{50}$ observed is Y(obs) of (a) MLR and (b) PLS methods.

and 6-31G basis set. The *in silico* analyses were conducted on a computer equipped with an processor intel@ core™ i7-12688 4.0 GHz, 8 core. The chemical shift value of ^{13}C-NMR for each method was compared with the experimental results to determine the most appropriate method for geometry optimization. Therefore, the descriptor of the optimized molecular structure was calculated using AlvaDesc software [40]. The 5666 topological descriptors were divided into 5 using the automatic linear modelling method in the SPSS software.

2.3. QSAR Model Development and Validation

The QSAR models were constructed using MLR and PLS statistical methods using IBM Statistics SPSS and Molegro Data Modeller (MDM) software [41][42]. The predictive value of the developed models was assessed using various validation techniques, including internal external validations and Y-randomization methods. In addition, we also assessed the applicability area (AD) of the MLR-derived QSAR model using the William plot to identify outliers [41]. Internal validation values were used, including $R^2_{training}$ (> 0.6), $R^2_{adjusted}$ (> 0.5), Q^2 (> 0.5), F_{cal}/F_{tab} (≥ 1), F-value (> 0.33), p-value (< 0.01), predicted residual error sum of squares [PRESS=Σ(predicted values – observed values)^2] < 0.2, standard error estimation (SEE) < 0.3, k (0,85 < k < 1,15), 'k' (0,85 < 'k' < 1,15). External validation values were used including R^2_{test} (> 0.6), Q^2_{F1} (> 0.5), Q^2_{F2} (> 0.5), R^2_m (> 0.5), ΔR^2_m (<0.2), concordance correlation coefficient (CCC) > 0.6, root mean square error prediction (RMSEP) < 0.3, $r_0^2 - r_0'^2$ (< 0,3), $\frac{r^2 - r_0^2}{r^2}$ (< 0.1), $\frac{r^2 - r_0'^2}{r^2}$ (< 0.1), Y-Randization (cRp^2) greater than 0.5 [41][43]–[45]. The validated statistical model predicted *Pf*DHFR-TS inhibitory activities of molecules that were neglected during model development. The best validated model was used to develop new molecules by replacing the R substituent using Cresset Spark software [46][47].

2.4. 3D-QSAR Analysis

Model analysis of molecular interaction fields (MIFs) using Open3DQSAR software (https://sourceforge.net/projects/open3dqsar/). The dataset was divided into 80% training set and 20% test set [48]. PLS analysis was used to establish a linear correlation between energy field as an independent variable and malaria activity as a dependent variable. Cross-validation using Leave-One-Out (LOO), Leave-Two-Out (LTO) and Leave-Many-Out (LMO) methods at 2.0 kcal/mol. The validation of the 3D-QSAR model included also the R^2 value, Structural Diversity-Enhanced Criteria (SDEC > 0.5), Standard Error of Estimate (SEE < 0.5), F-statistic (F > 3.84, α = 0.05), and Standard Deviation of Errors of Prediction (SDEP < 0.5). A high SDEC indicates sufficient structural diversity in the data set. A high SDEP value indicates greater variability in forecasts. The lower the SEE value, the better the model predicts biological activity. An F statistic value above 4 is often seen as an indication that the model is statistically significant. The best model obtained was validated based on the optimal number of components (N), which yielded cross-validation values of R^2 > 0.8 and Q^2_{LOO}, Q^2_{LTO}, and Q^2_{LMO} > 0.5 with a minimum standard error. Visualizing the interaction region with PyMOL.

2.5. ADME Properties, Prediction of Drug-likeness, Toxicity of Newly Developed Molecules

The absorption, distribution, metabolism, and

excretion (ADME) aspects are one of the stages that determine whether a drug molecule can be continued in clinical trials [49][50]. The ADME method is often known as the term drug pharmacokinetic prediction. The rules that *in silico* methods must follow to find chemical molecules that might be drugs are those of Lipinski [51], Ghose [52], Veber [53], Egan [54], Muegge [55], bioavailability score [56], and synthetic accessibility [57]. This study predicts the drug-like properties of highly active molecules and ensures their application to the developed QSAR model. This rule is based on the evaluation of the pharmacokinetic characteristics of drugs intended for human use. This rule helps in identifying drugs based on the 2D structure of the molecule and its bioavailability in the digestive tract [58]. The molecular structures that violate this rule have pharmacokinetic problems related to ADME. In addition, TPSA and n-rotB are also considered [59]. Based on these factors, we can determine whether the molecule interacts with flexible or inflexible receptors [60]. For ADME and drug-likeness prediction, we used several web servers and then took the average value of the measured parameters, including SwissADME [57], ADMETSAR [61], [62], Pre-ADMET [63], ADMETlab 3.0 [64], and pkCSM [65].

An analysis of the toxicity of the active substance should also be carried out to assess possible adverse reactions when administered orally. The toxicity analysis in silico was performed using ProTox 3.0 web server (https://tox.charite.de/protox3). The ProTox website serves as a virtual laboratory for predicting small molecule toxicity. Assessment of toxicity includes acute or oral toxicity, as well as organ toxicity and various parameters [66]. For the prediction of oral toxicity (LD_{50}) in rodent models, the classification of molecules toxicity according to the Global Harmonized System (GHS) is used. Toxic doses are often reported as LD50 values expressed in mg per kg of body weight. The LD_{50} indicates the dose at which 50% of test subjects die from exposure to the substance. ProTox 3.0 classifies substances into six different toxicity classes, including Class 1 ($LD_{50} \leq$

Table 3. Internal and external validations of 2D-QSAR models.

	Parameter	MLR	PLS	Threshold
Internal Validation	$R^2_{training}$	0.9406	0.9334	> 0.6
	$R^2_{adjusted}$	0.9539	0.9439	> 0.5
	Q^2	0.8720	0.8350	> 0.5
	F_{cal}/F_{tab}	4.7353	4.2735	≥ 1
	F-value	51.289	47.289	> 0.33
	p-value	0.0001	0.0001	< 0.01
	PRESS	0.0285	0.0321	< 0.2
	SEE	0.0520	0.0440	< 0.3
External Validation	R^2_{test}	0.9972	0.9916	> 0.6
	Q^2_{F1}	0.9929	0.9924	> 0.5
	Q^2_{F2}	0.9925	0.9912	> 0.5
	R^2_m	0.9220	0.9160	> 0.5
	ΔR^2_m	0.0069	0.0057	< 0.2
	CCC	0.9960	0.9910	> 0.6
	k	0.9975	0.9905	0,85 < k < 1,15
	k'	1.0025	1.0020	0,85 < k' < 1,15
	RMSEP	0.0174	0.0154	< 0.3
	$[r_0^2 - r'^2_0]$	0.04		< 0.3
	$[r^2 - r_0^2]/r^2$	0.08		< 0.1

Table 4. Y-randomization models.

Model	R	R^2	Q^2	Model	R	R^2	Q^2
Original	0.96996	0.94082	0.87156				
Rand 1	0.56675	0.32120	-0.35301	Rand 26	0.72120	0.52013	0.11404
Rand 2	0.44949	0.20204	-0.81016	Rand 27	0.42869	0.18377	-0.56028
Rand 3	0.39899	0.15919	-0.59589	Rand 28	0.58206	0.33879	-0.22309
Rand 4	0.08308	0.00690	-1.21169	Rand 29	0.69620	0.48470	-0.04763
Rand 5	0.37897	0.14362	-0.70695	Rand 30	0.45612	0.20805	-1.53705
Rand 6	0.53622	0.28753	-0.62526	Rand 31	0.37476	0.14045	-0.83421
Rand 7	0.20508	0.04205	-1.00567	Rand 32	0.34439	0.11860	-0.79099
Rand 8	0.57987	0.33625	-0.68983	Rand 33	0.56670	0.32115	-0.33625
Rand 9	0.42526	0.18084	-0.84253	Rand 34	0.30477	0.09288	-0.91651
Rand 10	0.50509	0.25511	-0.67622	Rand 35	0.74423	0.55388	0.07604
Rand 11	0.46185	0.21330	-0.31488	Rand 36	0.63524	0.40353	-0.13433
Rand 12	0.38523	0.14840	-0.70456	Rand 37	0.46868	0.21966	-0.70535
Rand 13	0.46227	0.21369	-0.64396	Rand 38	0.52617	0.27686	-0.52861
Rand 14	0.41006	0.16814	-0.58493	Rand 39	0.35265	0.12436	-0.61385
Rand 15	0.46302	0.21439	-0.70584	Rand 40	0.39381	0.15509	-0.93359
Rand 16	0.43890	0.19263	-0.79107	Rand 41	0.63009	0.39702	-0.20555
Rand 17	0.51459	0.26480	-0.26424	Rand 42	0.40960	0.16777	-0.94138
Rand 18	0.24371	0.05939	-0.90713	Rand 43	0.36864	0.13590	-0.54073
Rand 19	0.40306	0.16246	-0.63242	Rand 44	0.30410	0.09248	-1.01915
Rand 20	0.42428	0.18002	-0.89734	Rand 45	0.41308	0.17063	-0.44574
Rand 21	0.62684	0.39293	-0.13471	Rand 46	0.75184	0.56526	0.13938
Rand 22	0.65442	0.42827	-0.09829	Rand 47	0.60163	0.36196	-0.32403
Rand 23	0.43370	0.18809	-0.44649	Rand 48	0.36906	0.13620	-1.60355
Rand 24	0.33727	0.11375	-0.70275	Rand 49	0.66283	0.43935	-0.13601
Rand 25	0.50264	0.25265	-0.38656	Rand 50	0.50068	0.25068	-0.51038

Random Models Parameters
Average R : 0.469962354
Average R^2 : 0.239741321
Average Q^2 : -0.585828269
*cRp^2 : 0.823015070

* Y-randomization (cRp^2) greater than 0.5

5, fatal if swallowed), Class 2 ($5 < LD_{50} \leq 50$, fatal if swallowed), Class 3 ($50 < LD_{50} \leq 300$, toxic if swallowed), Class 4 ($300 < LD_{50} \leq 2000$, harmful if swallowed), Class 5 ($2000 < LD_{50} \leq 5000$, possibly harmful if swallowed), and Class 6 ($LD_{50} > 5000$, non-toxic) [67]. A higher toxicity class molecules have less of an impact on digestion. Among organ toxins are hepatotoxicity, neurotoxicity, nephrotoxicity, respiratory toxicity, and cardiotoxicity. Endpoint toxicity encompasses cytotoxicity, carcinogenicity, immunotoxicity, mutagenicity, blood-brain barrier permeability [67]. The active category suggests that the chemical has a great potential or activation to induce toxic

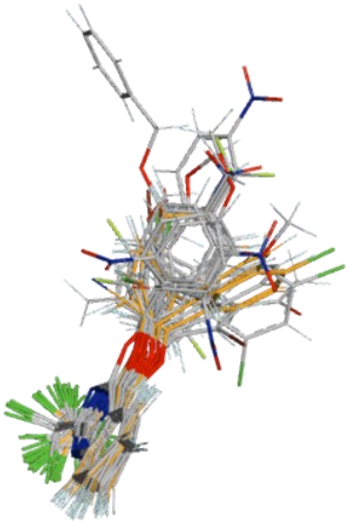

Figure 3. Molecular alignment of 26 datasets to molecule C30.

consequences on a given organ. Consequently, the molecule might endanger the operation of the pertinent organ by means of damage or impairment. The word "inactive" denotes that the chemical does not have much toxic potential for a given organ. Stated differently, the chemical is not expected to produce negative effects and is regarded as safe in the framework of toxicity to the organ under analysis.

2.6. Molecular Docking against Wild-Type (WT) and Quadruple Mutant (QM) PfDHFR-TS

The molecular docking studies were carried out on new 4-benzyloxy-2-trichloromethylquinazoline derivatives. It was compared with WT and QM-*Pf*DHFR-TS, where the protein database PDB ID was 3QGT from https://www.rcsb.org/structure/3QGT and 3JSU from https://www.rcsb.org/structure/3JSU, respectively. The target protein was produced using YASARA STRUCTURE version 23.5.19 software to separate the three-dimensional crystal structure and the native ligand. The parameters for redocking the grid box were set to 5.0 Å in a cube shape in accordance with the YASARA STRUCTURE protocol. The grid sizes x, y, z and alpha, beta, and gamma angles were 20.64, 20.64, 20.64 Å, and 90°, 90°, 90°, respectively. The molecular docking protocol using YASARA STRUCTURE's *dock_run.mcr* script. The receptor-ligand complex was redocked 1000 times with 25 iterations to validate the method, and the resulting ligand pose showed an RMSD value of less than 2 Å, suggesting a satisfactory confidence level [68][69]. Predicting the value of the binding constant (KD) is a crucial goal in computational chemistry because it saves time because the binding properties of a molecule can be evaluated without synthesis. It was determined from the calculation of the YASARA log file. Both K and ΔG° can predict the equilibrium ratio between product and reactants for a reaction. According to the equation, K is related to ΔG°. When $K > 1$ prefers equilibrium products to reactants. Standard Gibbs free binding energy ΔG° calculated according to Eq. 1 [70][71].

$$L + R \underset{k_{off}}{\overset{k_{on}}{\rightleftharpoons}} C$$

$$K_A = \frac{1}{K_D} = \frac{k_{on}}{k_{off}} = \frac{[C]}{[L]\cdot[R]}$$

$$\Delta G^0 = -RT \ln K_A \quad (1)$$

L, R and C stand for ligands, free receptor, complex, k_{on} and k_{off} are rate constants and K_A is the complex association constant. The most common measure of the bond strength of ligands is their inverse, the complex dissociation constant K_D. Analysis of molecular docking results using Discovery Studio Visualizer v24.1.0.23298, PyMOL 1.0, and Protein-Ligand Interaction Profiler web server (https://lip-tool.biotec.tu-dresden.de/plip-web/lip/index).

2.7. Molecular Dynamics Simulation

The results of the molecular docking of molecules S10, S23 and S64 were then subjected to

molecular dynamic simulations to determine whether the complex structure changed after they were perturbed by a group of H_2O molecules. The software used for the YASARA STRUCTURE simulation was the *md_run.mcr* script. The force field used in the simulation was AMBER14 with a simulation field of 10 Å, in particular the grid field dimensions (x, y, z) and the angles alpha, beta and gamma, which were set to the following values of 106.65, 106.65, 106.65, 90°, 90°, and 90°. The system was kept at a temperature of 310 K and a pressure of 1 atm (NPT ensemble) with a pH of 7.4 and 0.9% NaCl. The method of minimizing the energy of the system used the steepest descent method. The simulation was carried out for 100 ns with a time step of 2.0 fs. Simulation snapshots were saved at intervals of 100 ps. The Molecular mechanics Poisson-Boltzmann surface area binding energy (MM-PBSA), root mean square deviation (RMSD), radius of gyration (RoG), root mean square fluctuation (RMSF), changes in hydrogen bonds, and solvent-accessible surface area (SASA) emerged from the molecular dynamics simulation analysis [72].

3. RESULTS AND DISCUSSIONS

An accurate representation of the molecular structure is fundamental for the analysis of QSAR; thus, geometry optimization is quite important for the quality of the descriptors. An effective way to confirm the geometry of the molecule against experimental data is to compute proton NMR chemical shifts with the quantum chemistry approach. Recent studies have shown that DFT using the B3LYP function with a suitable baseline provides accurate results for predicting biological activity. Optimizing the geometry of the molecule using DFT has successfully improved the accuracy of QSAR compared to other methods [73]. According to previous work [74], in order to obtain data close to experimental results, the calculation of proton chemical shifts and geometry optimization are required. This requires a correct methodology and set of assumptions.

In this study, the geometric structure was validated by optimizing proton NMR shifts using DFT (B3LYP) with 3-21G, 6-31G, 6-31G+, 6-31G++, and 6-311G++ base sets. The method which is considered to be closest to the experimental results is the one with the lowest PRIMA value and the nearest proton NMR shift to the -R substituent, so that it may be used to optimize all molecules used in the QSAR analysis. The atomic number for the identification of the chemical shift is given in Table S1. The number of protons used to determine the chemical shift between the results of quantum chemical calculations and experimental results is the number of protons close to the -R substituent, namely H-8, H-9, H-10 and H-11. The H-10 is the proton closest to -R, so this proton determines whether the molecule geometry algorithm or other data sets are valid. The smallest PRESS indicates that the calculated value for the chemical shift of the protons is similar to the results of the ^{1}H-NMR [75]–[77] experiment, which is helpful when choosing the optimal DFT method. The PRESS value is the total difference between the experimental and the predicted ^{1}H-NMR shifts.

The results of the proton shift based on DFT quantum computation obtained that the H-10 proton with the B3LYP method and the 6-31G basis set had the same chemical shift value as the

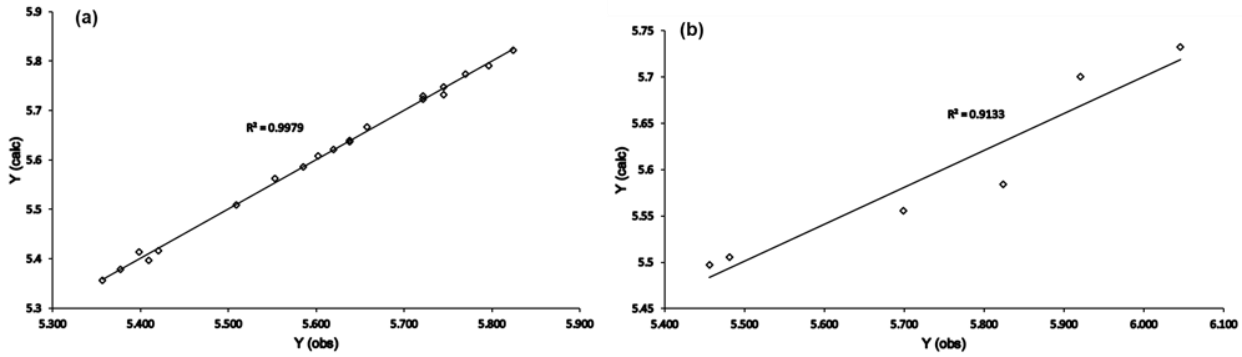

Figure 4. $Y_{(obs)}$ vs $Y_{(calc)}$, (a) training set dan (b) test set.

experimental results of 8.07 ppm. The PRESS value of 0.87 indicates that the dominant method used to optimize all molecules in the QSAR analysis is the B3LYP DFT method with the 6-31G basis set. Meanwhile, for the calculation of the proton NMR chemical shift value using the equation that can be seen on the page *http://cheshirenmr.info/Instructions.htm*. The intercept and slope values of the equation are obtained from the page *http://cheshirenmr.info/ScalingFactors.htm*.

The determining datasets using the 5:1 rule to avoid overfitting and data generalization. Based on this rule, the minimum number of datasets used is 25 molecules. The number of datasets considered to be in the valid category in this study was 27 molecules. In order to reduce randomization data in the HKSA analysis, the activity value of IC_{50} shall be converted into pIC_{50}. The 27 molecules are then divided into two groups of molecules in the dataset, namely 21 molecules used as a training set and the remaining 6 molecules used as a test set. The distribution of the datasets following the DTC-Lab rule, i.e., 80 % training sets and 20 % test sets.

3.1. Descriptor Selection and Model Accuracy

We performed the descriptor on 27 molecules of 4-benzyloxy-2-trichloromethylquinazoline derivatives using AlvaDesc standard parameters. The screening results obtained 5 descriptors, including three from the class of 2D autocorrelations with the codes ATS6m, ATSC7m, and GATS4e, respectively; one from the class of margin adjacency indexes with code (SpMax_AEA (ed)); and one from the class of 3D-MoRSE descriptors (Mor28e), shown in Table S2. The ATS6m and ATSC7m descriptors [78][79] are 2D-autocorrelation descriptors developed by Broto-Moreau. ATS6m refers to the "Average Shape Index", which measures the geometric similarity of molecules at the molecular level. It is often used to provide information about how complex or simple a molecular structure is compared to other molecules. It is calculated based on the geometry of the connection and its spatial properties. ATSC7m stands for "average topological shape characterization" of chemical molecules. It is a metric that is used to describe and refine the topological representation of a molecular structure in terms of its biological activity. Gats4e refers to

Table 5. MIFs contribution, internal and external validation of the 3D-QSAR models.

Model	Internal validation						External validation			Contribution (%)	
	R^2	SDEC	Q^2_{LOO}	Q^2_{LTO}	Q^2_{LMO}	SEE	F	R^2_{pred}	SDEP	SD on SDEP	Steric	Electrostatic
1	0.743	0.072	0.342	0.337	0.328	0.062	171.66				17.308	82.692
2	0.955	0.030	0.515	0.499	0.482	0.043	177.96	0.573	0.115	0.005	27.916	72.084
3	0.978	0.021	0.642	0.617	0.584	0.041	204.63	0.898	0.099	0.006	37.619	62.381
4	0.990	0.014	0.636	0.613	0.587	0.037	221.39	0.957	0.085	0.007	45.175	54.825
5	0.996	0.009	0.631	0.604	0.574	0.033	283.16	0.982	0.085	0.008	51.804	48.196

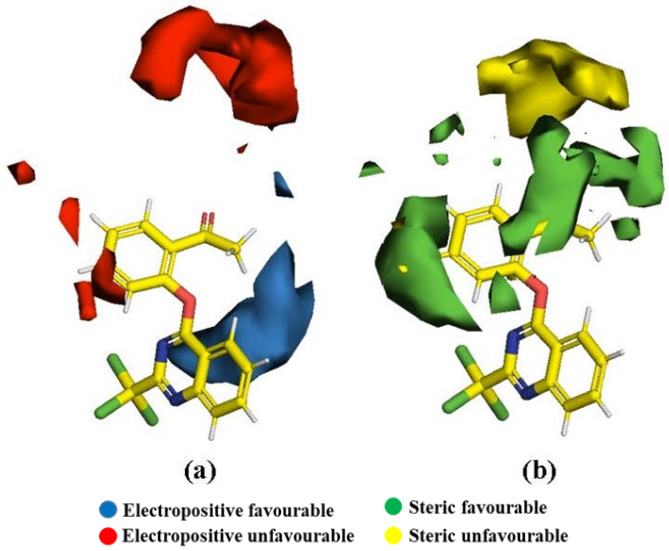

Figure 5. Open3DQSAR contour maps of 4-benzyloxy-2-trichloromethylquinazoline derivatives. (a) electrostatic contours and (b) steric contours.

"Geary Autocorrelation of Lag 4." This descriptor measures the autocorrelation of a specific property (e.g., polarity and charge) at a distance of four bonds within the molecular structure. Gats4e provides information on how such properties are distributed within a molecule and how they can influence its biological activity [79][80]. SpMax_AEA(ed) refers to Spanning Max Atom Electronegativity (ed). This descriptor measures the maximum electronegativity of atoms in a molecular structure, with a focus on atoms that are directly connected to each other within the bond network of the molecule. It determines the highest electronegativity value of an atom within the molecule. This is important to understand how the molecule interacts with biological targets, particularly with regard to ionic interactions and polarity [79][81]. refers to the "Molecular Connectivity Index," which is a measure of the disorder or complexity of a molecular structure based on connectivity between atoms. In particular, Mor28e calculates the connectivity of a molecule by taking into account the number of bonds connected to the atoms within that structure [79][82]. This descriptor provides an index that represents how atoms are connected together in the molecule. This is useful for assessing the potential reactivity and interaction of the molecule.

The cumulative accuracy of the multilinear regression model depends on the number of descriptors used to build the QSAR model. The model accuracy decreases sharply by 0.4046 when the number of descriptors is two. The model increases by 0.9335 when the number of descriptors rises to three and decreases slightly when 0.9113 is four descriptors. The model increases again by 0.9985 when the descriptors are five, as shown in Fig. S2, and then decreases further as the number of descriptors increases. Based on these results, five descriptors were used in the development of the QSAR model.

Table 2 shows the correlation matrix, variance inflation factor (VIF), and mean effect (MF) of the descriptors. Each descriptor pair has no intercorrelation if the Pearson correlation coefficient is less than 0.5 [45]. The VIF was calculated for each model descriptor and all values were between $1 < \text{VIF} \leq 5$ [41][83], which is a necessary requirement for approval of a developed model. We calculated the contribution of each individual model descriptor using MF. The descriptors ATS6m, ATSC7m, GATS4e, SpMax_AEA(ed), and Mor28e contributed to the model with values of 0.382 (15%), 0.375 (15%), 0.109 (5%), 1.339 (53%), and 0.308 (12%).

3.2. QSAR Applicability Domain (AD)

The scope of the QSAR model relates to the specific area within the chemical space in which the model can provide precise predictions as defined by the five previously defined model descriptors. This study uses the leverage approach to analyze the

Table 6. ADME properties of newly developed molecules.

Molecules	Absorption		Distribution		Metabolism							Excretion
					Substrate				Inhibitor			
					CYP							
	Intestinal absorption (human) Numeric (% Absorbed)	VDss (human) Numeric (log L/kg)	BBB permeability Numeric (log BB)	CNS permeability Numeric (log PS)	2D6	3A4	1A2	2C19	2C9	2D6	3A4	Total Clearance Numeric (Log ml/min/kg)
					Category (Yes/No)							
Chloroquine	89.929	1.901	0.722	-2.302	Yes	Yes	Yes	No	No	Yes	No	1.137
Doxorubicin	53.635	1.770	-1.767	-4.282	No	No	No	No	No	No	No	1.091
Doxycycline	37.262	0.596	-0.942	-3.867	No	No	No	No	No	No	No	0.350
Pyrimethamine	91.841	-0.004	-0.156	-2.148	No	No	Yes	No	No	No	No	-0.034
KA5*	82.658	-0.066	-1.112	-2.456	No	Yes	Yes	Yes	Yes	No	Yes	0.329
C30**	91.899	-0.162	0.166	-1.606	No	Yes	Yes	Yes	Yes	No	No	0.141
S10	93.309	1.088	0.590	-2.320	No	Yes	Yes	Yes	Yes	No	Yes	0.242
S23	89.809	0.528	0.529	-2.581	No	Yes	Yes	Yes	Yes	No	Yes	0.038
S64	89.562	0.616	0.355	-2.697	No	Yes	Yes	Yes	Yes	No	Yes	-0.085

* Native ligand of the target 3JSU
** The best ligand from original dataset

chemical space in Fig. 1, the Williams diagram and Cook distance were used to identify the reaction and structural outliers from the standardized residuals calculated using the leverage values for all molecules.

Interestingly, all molecules in the data set fall within the threshold for standardized residuals (σ = ± 2.5) or leverage (h^* = 0.782) [43]–[45] (Fig. 1 (a)). Moreover, observations were also made using the Cook distance measure, in which all molecules in the data set were also within the threshold of Cook's D < 1 [84][85] and standardized residuals (σ = ± 2.5) (Fig. 1(b)). Therefore, no structural outliers were found in the model, and these influential molecules can be used to develop prominent molecules with increased activities.

3.3. QSAR Analysis

Two QSAR model development techniques such as MLR and PLS were used in this work. The construction of these models depends on five significant descriptors, in particular ATS6m, ATSC7m, GATS4e, SpMax_AEA(ed), and Mor28e. Table S2 shows the contribution of each descriptor to increasing activity. Both descriptors ATS6m and ATSC7m are 2D autocorrelation classes that contribute negatively to increasing activity, while the 2D autocorrelation class Gats4e makes a positive contribution. As activity increases, the value of the Broto-Moreau log function of the ATS6m descriptor is less than 6 and ATSC7m is less than 7. The contribution of GATS4e is shown by a Sanderson electronegativity value of over 4. Both the SpMax_AEA(ed) and Mor28e descriptors from the class of edge adjacency indexes as well as the 3D Morse descriptors show a positive increase in activity. The QSAR model, which uses MLR and PLS, is provided in eq. 2 and eq. 3. The MLR and PLS equations show that the descriptors ATS6m and ATSC7m descriptors make a negative contribution, while the descriptors GATS4e, SpMax_AEA(ed), and Mor28e contribute positively to increasing the $p\mathrm{IC}_{50}$ value. Although the descriptor values ATS6m, ATSC7m, and SpMax_AEA(ed) appear to be significantly different in both equations, they have no effect on the R^2_{training} and R^2_{test} forecast values. Both equations show that the $p\mathrm{IC}_{50}$ is linearly related to the parameters GATS4e, SpMax_AEA(ed), and Mor28e, while it is inversely proportional to the parameters ATS6m and ATSC7m.

$$(p\mathrm{IC}_{50})_{\mathrm{MLR}} = -3435.4170 - 1.527\times\mathrm{ATS6m} - 0.0062\times\mathrm{ATSC7m} + 1.7604\times\mathrm{GATS4e} + 169.3426\times\mathrm{SpMax\_AEA(ed)} + 1.2049\times\mathrm{Mor28e} \quad (2)$$

$$(p\mathrm{IC}_{50})_{\mathrm{PLS}} = -1312.7684 - 0.3112\times\mathrm{ATS6m} - 0.0121\times\mathrm{ATSC7m} + 0.5707\times\mathrm{GATS4e} + 185.0384\times\mathrm{SpMax\_AEA(ed)} + 0.5793\times\mathrm{Mor28e} \quad (3)$$

Equation 2 can be rewritten in a simple eq. 4 form as:

Table 7. Drug-likeness prediction of newly designed molecules.

Molecules	Drug-likeness parameters						
	Lipinski	Veber	Egan	Muegge	Ghose	Bioavailability score	Synthetic accessibility
Chloroquine	Yes	Yes	Yes	Yes	Yes	0.55	2.76
Doxorubicin	No	No	No	No	Yes	0.17	5.81
Doxycycline	Yes	No	No	No	Yes	0.11	5.25
Pyrimethamine	Yes	Yes	Yes	Yes	Yes	0.55	2.43
KA5*	Yes	Yes	Yes	Yes	Yes	0.55	2.54
C30**	Yes	Yes	Yes	Yes	Yes	0.55	2.67
S10	Yes	Yes	Yes	Yes	Yes	0.55	2.67
S23	Yes	Yes	Yes	Yes	Yes	0.55	2.66
S64	Yes	Yes	Yes	Yes	Yes	0.55	2.70

* Native ligand of the target 3JSU
** The best ligand from original dataset

Table 8. Toxicity prediction results using ProTox web server.

Molecules	Oral toxicity		Organ Toxicity and endpoints									
	LD_{50} Predicted (mg/kg)	Toxic Class	A	B	C	D	E	F	G	H	I	J
Chloroquine	750	4	X	√	X	√	X	X	√	√	X	X
C1	500	4	X	√	X	X	X	X	X	X	X	√
C30	1000	4	X	√	X	X	X	X	X	X	X	√
CP6	92	3	X	√	X	√	X	X	X	X	X	√
KA5	1000	4	X	√	X	√	X	√	√	√	√	√
S10	600	4	X	√	X	√	X	X	X	X	X	√
S23	500	4	X	√	X	√	X	X	X	X	X	√
S64	388	4	X	√	X	√	X	X	√	X	X	√

A) Hepatotoxicity B) Neurotoxicity C) Nephrotoxicity D) Respiratory toxicity E) Cardiotoxicity
F) Carcinogenicity G) Immunotoxicity H) Mutagenicity I) Cytotoxicity J) BBB-barrier
√ = active, X = inactive, red = highly active, green = totally inactive

$$(pIC_{50})_{MLR} = K + \Sigma\,(c_i \,.\, X_i) \qquad (4)$$

where K is a constant of -3435.4170, c_i is the coefficients of various parameters, and X_i are the values of the variables involved in the model (X_1 = ATS6m, X_2 = ATSC7m, X_3 = GATS4e, X_4 = SpMax_AEA(ed), X_5 = Mor28e). The same can also happen in equation 3. The predictability of the model was high due to low residual values, and most low residual values were found in the MLR method and not in the PLS. The residual values of observed $Y_{(obs)}$ and predicted $Y_{(calc)}$ from 27 data sets of 4-benzyloxy-2-trichloromethylquinazoline derivatives obtained using the MLR and PLS methods are presented in Table S3.

Fig. 2 shows the linear relationship between observation $Y_{(obs)}$ and predicted $Y_{(calc)}$ from the test (red) and training (black) sets using MLR and PLS. The $R^2_{training}$ and R^2_{test} values for the MLR method are 0.9406 and 0.9972, respectively; and the $R^2_{training}$ and R^2_{test} values for the PLS method are 0.9334 and 0.9916, respectively. The $R^2_{training}$ value for the MLR method is slightly higher than the PLS, but there is no significant difference in the number of ballots. The validation capability of both models is said to be good, as they have a R^2_{test} value that is not too different from $R^2_{training}$ and can meet the internal and external validation thresholds > 0.6. Moreover, the R^2_{test} is higher than the $R^2_{training}$ indicating that both models are capable of predicting new data well and do not overfit and that the model has a good generalization capability. If the model is overfitting, it means that it fits the training data too well, so that its performance is good for the training data but poor for the test data (validation).

The QSAR model was validated both internally and externally using criteria such as $R^2_{training}$, $R^2_{adjusted}$, Q^2, F_{cal}/F_{tab}, F-value, p-value, PRESS, SEE, R^2_{test}, Q^2_{F1}, Q^2_{F2}, R^2_m, ΔR^2_m, CCC, RMSEP, and the Golbraikh-Tropsha validation. The QSAR model meets internal and external thresholds for statistical validation. Table 3 shows that both MLR and PLS models are predictive. In this study, we selected the MLR model to develop new *Pf*DHFR-TS inhibitor molecules from 4-benzyloxy-2-trichloromethylquinazoline derivatives.

Y-randomization is one of the external validation tests of a model to determine whether the observed relationship between chemical structure and biological activity is real and predictive or merely coincidental. Table 4 shows the results of 50 Y-randomization iterations (randomization from random 1 to random 50) performed on the QSAR model. The R, R^2 and Q^2 secretarial values were calculated for each iteration. In addition, the average values of R, R^2 and Q^2 of all Y-randomization models were also calculated, as well as cRp^2. The original model has very high R values (0.96996) and R^2 values (0.94082), almost equal to 1. This suggests a very good plausibility of the data on the training topic. The Q^2 value (0.87156) is also high, indicating a seemingly good predictive power.

R, R^2 and Q^2 values vary significantly between 50 Y randomization models. This is important because differentiation of Y violates the integrity of true relationships. differentiation of ignorance. The average R of the random models (random 1 to random 50) is 0.46996, much lower than the original model. This value indicates that random modeling cannot explain the relationships present in the data set. An even lower average R^2 (0.239714321) generally confirms that Y-randomization models do not have sufficient predictive power. The average Q^2 obtained by random models (0.58828629) is rather low, which highlights the fact that random models are not very good at predicting new data. The high cRp^2 (0.82301507) indicates that the QSAR model validated is very good and robust. Validation results of Y-randomization strongly support the validity of the original QSAR model. The original QSAR model does not adequately represent the data on tuition. The model really captures the fundamental relationship between descriptors (X) and biological activity (Y). The correlation found in the original model is no accident. There is a real and predictive relationship between structure and action. The original QSAR model has the potential to accurately predict the activity of novel molecules.

Table S4 shows the structure of new 4-benzyloxy-2-trichloromethylquinazoline derivatives and the MLR-QSAR estimated activity values for 26 molecules. New substitution structures have been identified using Spark database to detect bio-isosteric substitution loss succinctly [86]. The chemical structures of 4-[(quinolin-2-yl)methoxy]-2-(trichloromethyl)quinazoline (S10), 4-[(1*H*-indol-6-yl)methoxy]-2-(trichloromethyl)quinazoline (S23), and 3-methyl-4-(((2-(trichloromethyl)quinazolin-4-yl)oxy)methyl)phenol (S64) were selected for ADME, drug-likeness and toxicity analysis because they had the best predicted IC_{50} values.

3.4. 3D QSAR Analysis and Functional Electron Density Approach

A 3D-QSAR analysis based on molecular interaction fields (MIFs) and electron density functionals was carried out to strengthen the classic QSAR predictions when determining the position of new substituents. MIFs are a concept that is used to describe the interaction between molecules and biological targets, taking into account steric and electrostatic aspects. MIFs map these parameters in a three-dimensional grid to evaluate how the size, shape, and charge distribution of a substituent can influence the interaction with the active site. Through this analysis, researchers can understand the effects of steric hindrance and the potential electrostatic energy of structural changes, which is very helpful when developing new molecules. Based on the information obtained, MIFs make it possible to develop substituents that are expected to increase biological activity and thus accelerate the drug development process. Electron density functional is an approach that uses the distribution of electron density in a molecule to understand the chemical properties and interactions between atoms. This approach is able to predict properties such reactivity and stability of molecules by calculating the electron density (ρ) and applying an energy functional that describes the energy of the system depending on this density. By means of different configurations to identify the most stable form, this principle allows scientists to assess the effect of substituent changes on chemical properties and reactivity and consequently optimize the structure of new molecules.

The data set for the superposition or molecular

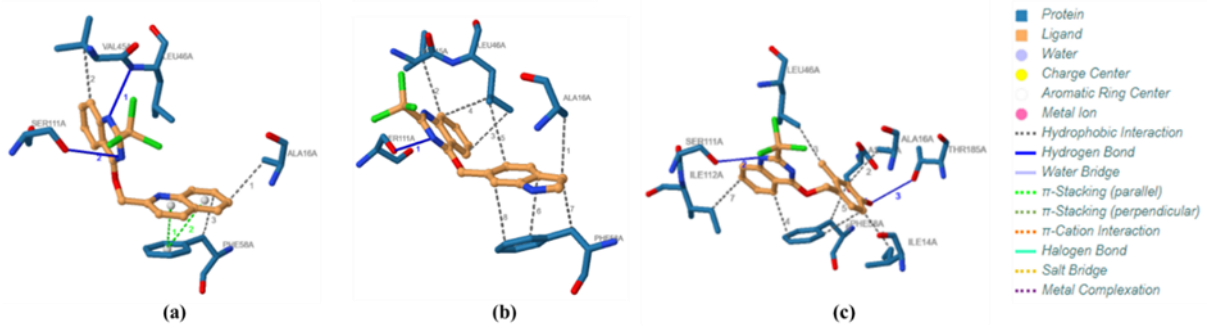

Figure 6. Interactions of (a) S10, (b) S23, and (c) S64 in the QM-*Pf*DHFR-TS (3JSU) binding pocket.

Table 9. The binding energy (ΔG), dissociation constant (K_D) and residue contacts of S10, S23, and S64 in the 3JSU binding pocket.

Molecule	Binding Energies (ΔG) kcal/mol	Dissociation Constant (K_D) μM	Contact Residues in the binding pocket
S10	-9.869	583	*H-bond*: Leu46, Ser111 *Hydrophobic*: Ala16, Val45, Phe58 *π-stacking*: Phe58 *Other hydrophobic*: Ile14, Cys15, Leu40, Gly41, Gly44, Trp48, Asp54, Met55, Asn108, Ile112, Pro113, Leu164, Tyr170
S23	-9.589	93.6	*H-bond*: Ser111 *Hydrophobic*: Ala16, Val45, Leu46, Phe58 *Other hydrophobic*: Ile14, Cys15, Leu40, Gly41, Gly44, Trp48, Asp54, Met55, Tyr57, Thr107, Asn108, Ile112, Pro113, Leu164, Gly166, Tyr170, Thr185
S64	-9.565	87.5	*H-Bond*: Asp54, Ser111, Thr185 *Hydrophobic*: Ile14, Ala16, Leu46, Phe58, Ile112 *Other Hydrophobic*: Cys15, Leu40, Gly41, Val45, Trp48, Met55, Tyr57, Asn108, Pro113, Leu164, Gly166, Tyr170

orientation of the reference molecule C30 aims to ensure a uniform conformation between different molecules, allowing a more accurate analysis of the relationship between structure and biological activity. This orientation helps identify critical interactions, improves model accuracy by reducing variability due to differences in orientation, and enables better interaction modelling. In addition, molecular orientation reduces noise in the data and allows direct comparisons between molecules to identify structural patterns related to activity. Molecular orientations therefore support the design of new molecules that are more efficient. Fig. 3 shows that all records are stacked on top of each other; in other words, there is no significant difference in the main structure.

Fig. 4(a) illustrates that the data points exhibit a strong correlation between $Y_{(obs)}$ and $Y_{(calc)}$, as they are inclined to form a straight line at a 45° angle (ideal line). The R^2 value of 0.9979 suggests a robust relationship in which the model may be responsible for almost all of the data variability. This implies that the model can highly accurately predict the biological activity of the molecules contained in the training set and has been well adjusted. There is a slight difference in Fig. 4(b). The R^2 value of 0.9133 indicates that the model is less effective in predicting the biological activity of invisible data, even though there is still a positive correlation between $Y_{(obs)}$ and $Y_{(calc)}$. The regression line does not exactly match the 45° line. Although the correlation is still strong, the lower R^2 value suggests a possible overadjustment in the training set, in which case the model might have acquired some patterns from the training data that do not completely apply to the test set. This emphasizes the need of general testing of 3D-QSAR models to ensure their accuracy outside of training data and cross-valuation.

The contribution of MIFs and the results of internal and external validation for five 3D-QSAR models are presented in Table 5 of the

Open3DQSAR analysis. Overall, the R^2 value rises from 0.743 in model 1 to 0.996 in model 5, which indicates a significant improvement in the accuracy of predicting biological activity. The 3D-grid spacing of the models were set to 1.0 Å. Based on internal validation, model 5 was identified as the best 3D-QSAR model for predicting the MIFs of new connection structures. Validation indices such as Q^2_{LOO}, Q^2_{LTO} and Q^2_{LMO} show similar improvements to the SEE decrease, indicating that the predictions of the model are increasingly accurate. The higher F-statistic also points to models that are more statistically significant. In the contribution analysis, the steric factor increasingly dominates from 17.308% (model 1) to 51.804% (model 5), while the contribution of the electrostatic factor falls from 82.692% to 48.96%. This shift suggests that as the model improves, there is a transition to focusing on steric interactions when predicting biological activity. This highlights how important it is to consider steric factors when developing new molecules, resulting in better models for 3D-QSAR analysis.

Fig. 5 shows electrostatic and steric contour maps for 4-benzyloxy-2-trichloromethylquinazoline derivatives. Fig. 5(a) shows the electrostatic contour map of the distribution of charges around the molecule, where blue indicates electropositive favourable areas that enhance interactions with negative targets, and red indicates electropositive unfavourable areas that may interfere with such interactions. Fig. 5(b), the steric contour map highlights the spatial arrangement, with green indicating sterically favourable areas promoting efficient interactions and yellow indicating sterically unfavourable areas inhibiting them. An analysis of both contour maps allows scientists to identify beneficial changes to improve biological activity while minimising undesirable interactions, and thus facilitates the development of new molecules. These results support the determination of substituents for the three new molecules listed in Table S4.

Fig. S3 shows the analysis of the electron density function of molecules S10, S23, and S64, which can be linked to the contour maps in Fig. 5, which show steric and electrostatic contours. The results of this electron density functional analysis reflect the predictions made using the steric and electrostatic contour maps in Fig. 5. The sterically favorable and electropositive contours shown in Fig. 5 indicate areas where effective interactions with biological goals can be expected. In Fig. S3, the green areas in molecules S10, S23, and S64 highlight areas of high

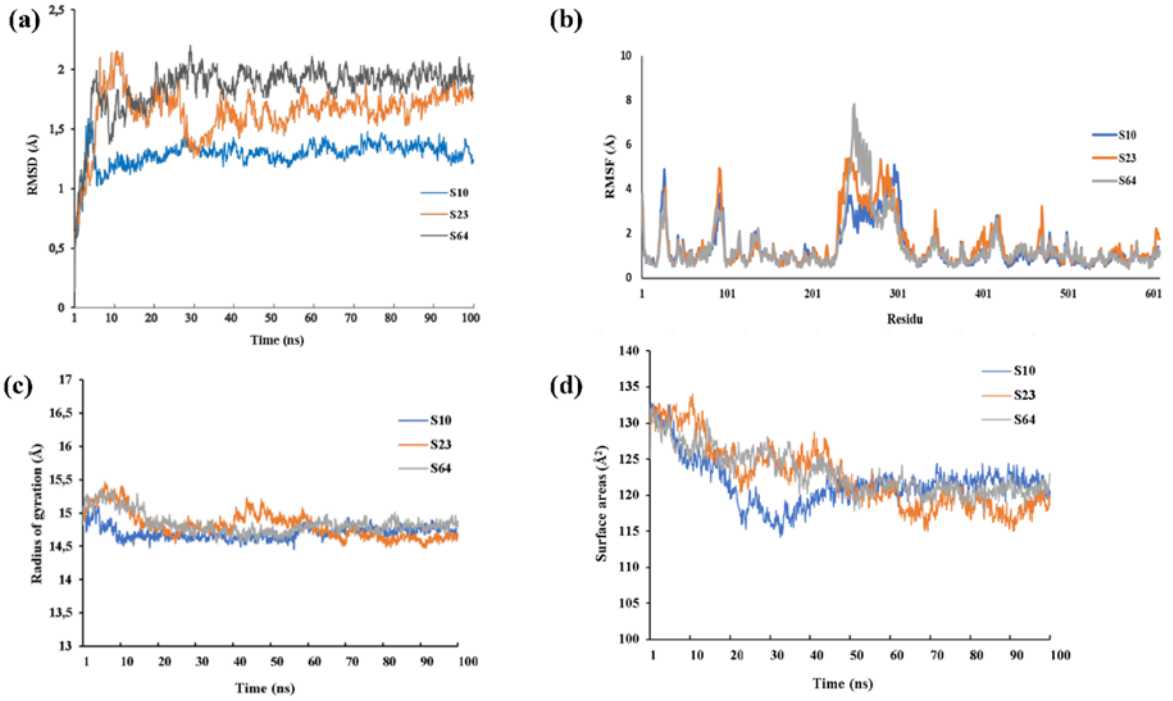

Figure 7. Graph of (a) RMSD, (b) RMSF, (c) RoG and (d) SASA values of complex S10-3JSU, S23-3JSU and S64-3JSU.

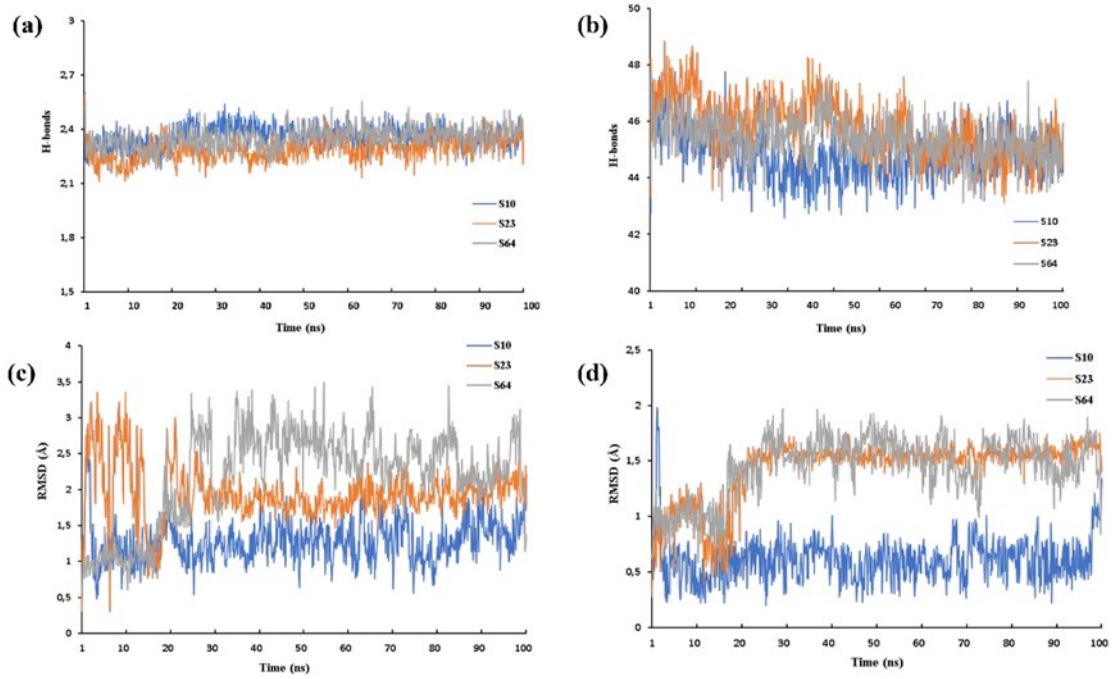

Figure 8. Graphs of (a) changes in hydrogen bonds (H-bonds), (b) hydrogen bond interactions in the binding pocket, (c) RMSD value of molecule movement in the binding pocket and (d) RMSD value of molecule conformation (superposition) with respect to native ligands.

electron density, reflecting the presence of electropositive favorable zones. Similarly, the distribution of green and red in these molecules illustrates the presence of sterically favorable areas based on the contours shown in Fig. 5. In other words, the visual results from Figure S3 support the predictions from Fig. 5, where the green areas in the molecules indicate potential positive interactions in the previously analyzed regions.

Furthermore, the analysis of the electron density in the molecules in Figure S3 shows green areas that reflect high electron density, which indicates electropositive favorable properties. This supports strong positive interactions with biological targets, which is consistent with the predictions from the contour maps in Fig. 5. Therefore, the substituent selection in molecules S10, S23 and S64 appears both appropriate and strategic, which results in better interactions based on the analyses from both figures.

3.5. ADME, Drug-likeness and Toxicity Prediction

Drug-likeness was used to evaluate qualitative properties and determine whether drugs could develop from novel molecules. The online tools pkCSM and SwissADME were used to predict ADME and drug similarities in silico, are presented in Tables 6 and 7. Absorption values above 30% indicate good intestinal absorption; all new molecules exceed 80%. LogVDss < 0.15 indicates low volume of distribution (VDss), and logVDss > 0.45 indicates high. Molecules S10, S23, and S64 exhibit favorable drug distribution throughout the body. A molecule with a log blood brain barrier (BBB) < -1 has poor brain distribution, while log BBB > 0.3 can cross BBB. Log PS > -2 can penetrate the central nervous system (CNS) and LogPS < -3 is challenging to move. Thus, S10, S23, and S64 have great potential to cross barriers.

ADME prediction helps to understand how a substance will act in the body, including how well it will be absorbed, distributed to target tissues, metabolised and eliminated. Meanwhile, drug similarity prediction assesses how similar a molecule is to existing drugs based on certain physical properties. ADME and drug similarity prediction results may be used to identify and modify the chemical structure of a molecule to improve its pharmacokinetic and pharmacodynamic profile. This may increase the effectiveness of the medicine, reduce the side effects and improve overall safety. The drug is biotransformed in the

body to form metabolites which may alter its effects and properties. Over 90% of drugs are biosynthesized in the liver, where the CYP1A2, CYP3A4, CYP2C19, CYP2D6 and CYP2C9 enzymes are vital for drug metabolism. Reducing these enzymes helps to raise blood drug concentrations. CYP2C19 and CYP3A4 are the main cytochrome P450 isoforms. Found to be CYP3A4 substrates and CYP3A4 and CYP2C19 inhibitors were the S10, S23 and S64. The total clearance value is the ratio of the concentration of the drug to the rate of elimination in the body, where a low value indicates accumulation of the drug. Predicting results showed that only molecules S23 and S64 were difficult to eliminate by liver and kidney.

Three molecules, S10, S23 and S64, showed a very good drug-likeness profile meeting all criteria: Lipinski, Veber, Egan, Muegge and Ghose. This suggests that these molecules have physicochemical properties that strongly support their potential as an oral medicinal product. All three also share the same bioavailability score of 0.55. This implies a relatively good prediction of absorption by the body. The values of their synthetic accessibility are also very similar, ranging from 2.66 to 2.70. This indicates that they are relatively easy to synthesize. Overall, S10, S23, and S64 have drug-likeness profiles comparable to CP6, KA5, C30, and chloroquine, indicating that all three have equally good potential as drug candidates.

The prediction results presented in Table 8 show that the predicted LD_{50} of molecules in the study ranged from 300 to 1,000 mg/kg. According to the toxicity assessment scale, where the LD_{50} ranges from 300 to 1,000 mg/kg, a molecule is classified as toxic level 4 and three molecules studied, S10, S23 and S64, fall within this category. This means that there is a risk of toxicity if swallowed, but not fatal (moderate toxicity). There is a difference in CP6 where the predicted LD_{50} of 92 mg/kg is in the level 3, toxic when swallowed.

Regarding organ toxicity and endpoints, the three molecules predicted are on average active in hepatotoxicity, respiratory toxicity, and BBB barrier. S10 and S23 are inactive in hepatotoxicity, nephrotoxicity, cardiotoxicity, carcinogenicity, immunotoxicity, mutagenicity, and cytotoxicity, respectively. S64 shows slightly active properties in neurotoxicity, respiratory toxicity, and immunotoxicity. If the toxicity prediction indicates high activity, the molecule is considered very toxic to a particular organ. Conversely, if completely inactive, the predicted molecule is not toxic to that organ. Based on the toxicity results, the three predicted molecules have moderate toxicity to non-toxic properties, starting with S23, followed by S10 and S64.

3.6. Molecular Docking

The validation procedure involves the re-docking of the native ligand to the active site of its target protein. This is to verify that the docking software and parameters used can reproduce the position of ligand binding as observed in the crystal structure of the protein. The success of the re-docking is usually evaluated by comparing the position of the re-docked ligand in the crystal structure with the position of the native ligand using the RMSD. Fig. S4 shows the results of re-docking KA5 in the 3JSU binding pocket. The native ligand before re-docking shall be represented in yellow and the native ligand after re-docking shall be represented in green. The RMSD value of re-docking was obtained as 0.6796 Å, indicating that the docking protocol successfully reproduced the binding position of the native ligand. The re-docking protocol used successfully validated the docking method, because the RMSD value obtained was within the acceptable range of < 2 Å. This indicates that the software and molecular docking parameters used in this study are reliable for further docking studies with other ligands that potentially interact with the target protein.

The interactions of molecules S10, S23, and S64 with amino acid residues in the 3JSU binding pocket are presented in Figure 6. The interactions with these mutants are interesting, as molecule S10 establishes two hydrogen bonds: one between the nitrogen atom (donor) of residue Leu46 and a hydrogen atom (acceptor) of a cyclic nitrogen in the parent structure of 2-trichloromethylquinazoline, measuring 2.28 Å, and the other between the nitrogen atom (donor) of residue Ser111 and another hydrogen atom (acceptor) of a cyclic nitrogen in the same parent structure, measuring 2.35 Å, as illustrated in Fig. 6(a). Additionally, there exist two P-type π-stacking interactions between the benzene ring of residue Phe58 and the

pyridine (3.99 Å) and benzene (3.14 Å) substituent rings. In addition to forming a π-stacking bond, the Phe58 residue also forms a hydrophobic interaction of 3.67 Å. Other hydrophobic interactions are Ala16 one bond and Val45 one bond between 3.39 and 3.68 Å.

Fig. 6(b) shows that there is one hydrogen bond formed between the oxygen atom (donor) of the Ser111 residue and the hydrogen atom (acceptor) of the nitrogen atom number 3 in the pyrimidine structure at a distance of 2.47 Å. Meanwhile, hydrophobic interactions are formed at the Ala16 residue as much as one bond, Val45 one bond, Leu46 three bonds, and Phe58 three bonds with a distance range of 3.45–3.96 Å. S64 interacts with amino acid residues in the 3JSU pocket and forms three hydrogen bonds, the first of which is between the oxygen atom (donor) of the Asp54 residue and the hydrogen atom on the phenol substituent (acceptor) which is at a distance of 2.66 Å. The second is between the oxygen atom (donor) of the Ser111 residue and the hydrogen atom (acceptor) of nitrogen number 1 of the pyrimidine structure which is 2.62 Å away. The third interaction occurs between the oxygen atom (donor) of the Thr185 residue and the hydrogen atom (acceptor) on the phenol substituent, which is situated 2.89 Å apart, as illustrated in Fig. 6(c). Furthermore, hydrophobic interactions occur with residues Ile14 (3.36 Å), Ala16 (3.53 Å), Leu46 (3.53 Å), Phe58 (3.50, 3.60, and 3.85 Å), and Ile112 (3.57 Å).

The predicted three-dimensional (3D) contours of hydrogen bonds in the first row and hydrophobic interactions in the second row for the three molecules in the 3JSU binding pocket are depicted in Fig. S5. The hydrogen bond donor area is shown in the pink contour while the green contour is the hydrogen bond acceptor area. In the first row, the hydrogen bond donor and acceptor areas of the amino acid residues in the 3JSU binding pocket are found widely in the three molecules. Similarly, in the second row, the hydrophobic interaction area is found in the three molecules. The three molecules are dominated by the positive hydrophobic interaction area which is marked in brown.

The binding energy between molecules S10, S23 and S64 with 3JSU is presented in Table 9. The energy was obtained from the results of molecular docking analysis using YASARA STRUCTURE software. Molecule S10 has the highest binding energy of -9.869 kcal/mol followed by S23 and S64 which are -9.589 and -9.565 kcal/mol, respectively. The K_D value of the 3JSU complex is consistent with the binding energy values of the three molecules. Molecule S10 shows a K_D strength of the 3JSU complex of 583 µM, while molecules S23 and S64 follow with 93.6 and 87.5 µM, respectively. Based on the residue contact parameters, molecules S64 and S10 show more hydrogen bond contacts in the 3JSU binding pocket

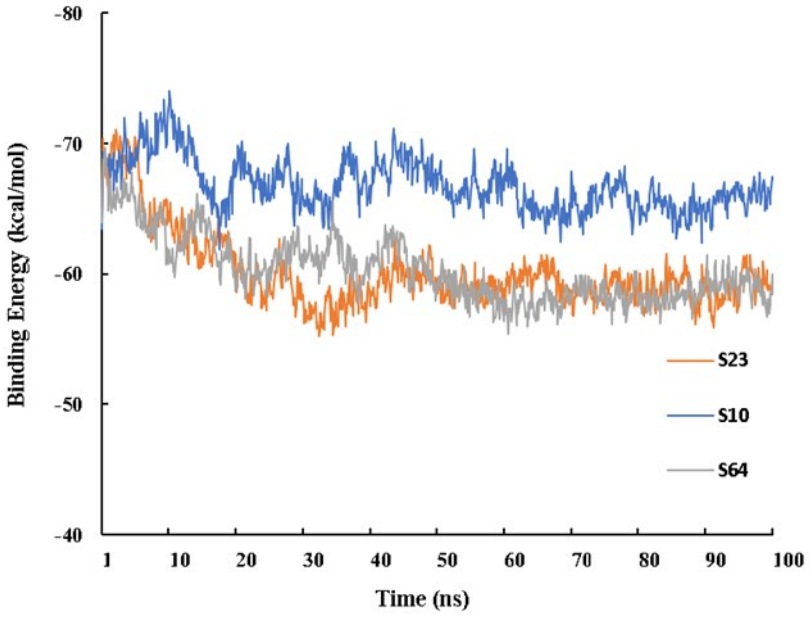

Figure 9. Binding energy values (MM/PBSA).

than S23. Amino acid residues Leu46, Asp54, Ser111, and Thr185 play important roles in the strength of *Pf*DHFR-TS ligand-receptor interaction. In addition, S10 also has a π-stacking bond, which increases the strength of the complex conformation.

The inhibition constant (K_i) on DHFR enzymes of *P. falciparum* Wild type (WT-*Pf*DHFR) and quadruple mutant (QM-*Pf*DHFR) and human (hDHFR) against Cycloguanil, Pyrimethamine, WR99210, KA5 [6][87] S10, S23, and S64 presented in Table S5. According to the inhibitor activity (K_i) values, molecules S10, S23, and S64 are effective inhibitors of both WT and QM *Pf*DHFR-TS enzymes. The results indicated that molecules S10, S23, and S64 exhibited a significant binding affinity for both WT *Pf*DHFR-TS (K_i = 0.46 ± 0.08 nM; 0.44 ± 0.41 nM; and 0.30 ± 0.39 nM) and QM *Pf*DHFR-TS (K_i = 45.99 ± 66.39 nM; 144.90 ± 67.48 nM; and 261.59 ± 68.40 nM), exceeding the binding affinity of pyrimethamine and cycloguanil. Although still lower than KA5, S10 and S23 molecules were more selective than KA5 due to their high human/plasmodium K_i ratios of 22.17 and 23.18, respectively.

3.7. Molecular Dynamics Simulation

The results of molecular docking analysis showed that the three candidate molecules of *Pf*DHFR-TS inhibitors were active on the mutant target. In order to test the stability of the complex resulting from the molecular docking, molecular dynamics simulations were performed using the addition of H_2O molecules as solvent. The simulation time for each complex was carried out at 100 ns and a temperature of 310 K using the Amber14 force field.

Fig. 7(a) shows that molecules S10 and S64 have relatively stable RMSD values below 2 Å after 20 ns. This indicates that both molecules have reached equilibrium and structural stability. Molecule S23 shows more fluctuations than S10 and S64; its peak is higher than 2 Å at about 30 ns, hence indicating more conformational changes or instability. While S23 may show more flexibility in this simulation, the lower RMSD values show that molecules S10 and S64 are more stable. Fig. 7(b) shows the RMSF fluctuations across residues, so indicating the stability or flexibility of every part of the protein or molecule structure. Since S23 shows many fluctuation peaks over several residues, implying that this molecule has more flexible or susceptible areas to conformational changes, S10 shows minimum fluctuations for most residues. The RMSF variation of S64 is inconsistent, yet it is typically not significantly distinct from that of S10. This suggests that certain residues are also quite stable, despite the presence of some significant fluctuations in specific regions. Residues with high RMSF values could be more flexible or unstable in response to environmental changes, so affecting either biological activity or ligand interactions. Conversely, residues showing low fluctuations are more inclined to improve the general stability of the structure. RoG shows the change in value related to the density of the structure over the simulation time. Lower RoG values indicate a more compact structure; higher RoG values may indicate more flexibility or structural expansion. While S23 shows more variation relative to S10, suggesting that this molecule may undergo more severe conformational changes as well as become less rigid over time, S10 shows minimal variation and remains constant around an identified value. S64 shows a similar RoG value to S10, but also shows some fluctuations in density as seen in Fig. 7(c). This suggests that S64 tends to be stable, but there are times when the structure can be more open. The stable RoG of S10 and S64 suggests that both tend to maintain a more compact form, which could have positive implications for their functional stability. S23 with larger fluctuations could indicate a wider interaction potential or higher reactivity, but also a risk of instability. SASA shows changes in values related to the surface exposure of the molecule to solvent. Higher SASA values indicate more molecules are exposed to solvent, while lower SASA values indicate more restricted areas. Fig. 7(d) shows S10 with relatively low and stable fluctuations, indicating that this structure tends to maintain solvent-accessible surface areas, with little change over time. S23 shows an increase in the SASA of this molecule likely more exposed to solvent over time, due to a tendency for more active conformational changes or structural relaxation. S64 shows a similar pattern to S10, with relatively stable SASA values. However, in some periods, there are fluctuations indicating varying surface exposure. The stable SASA of S10 and S64

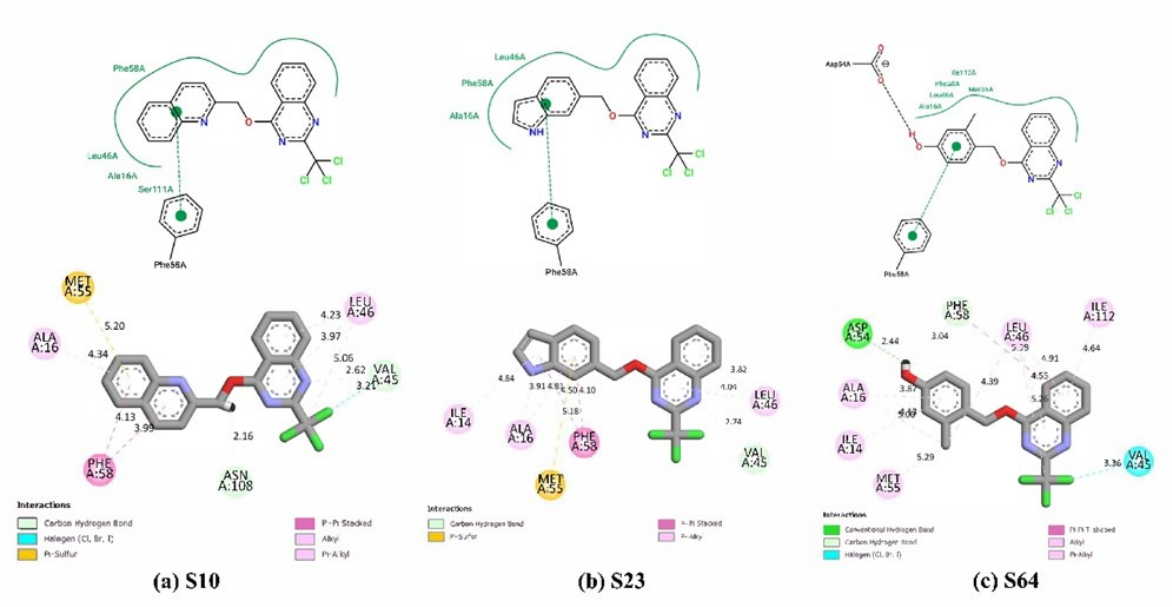

Figure 10. Interaction of molecules (a) S10, (b) S23 and (c) S64 in the binding pocket of the target mutant (3JSU) after molecular dynamics simulation (100 ns).

suggests that these two molecules may be more efficient in interacting with other molecules compared to S23. The increased SASA of S23 may also indicate higher reactivity but may also indicate greater instability.

Fig. 8(a) shows that all three molecules have a stable trend in the number of hydrogen bonds over the simulation time. The number of hydrogen bonds fluctuates slightly, but there is no significant change indicating that all molecules maintain their proximity to their ligands over the simulation time. Molecule S10 appears to have a slightly higher and more consistent number of hydrogen bonds than the others. This may indicate that S10 interacts better in the context of hydrogen bonds. S23 shows a larger fluctuation in the number of hydrogen bonds than S10 and S64. This may indicate fewer stable interactions. However, not as many as S10 at any one moment, the count of hydrogen bonds in S64 seems to be comparable to S10. Though the three molecules vary, the hydrogen bonds that might influence their molecular interactions across the simulation period show no appreciable change. Fig. 8(b) shows that the hydrogen bond interactions of all three molecules vary over time, but S10 and S64 show better stability than S23. Stable interactions are important to ensure that molecules can bind ligands effectively in a biological context. S10 shows high consistency in the number of hydrogen bond interactions throughout the simulation time, with little fluctuation. This indicates that S10 has stable interactions with the binding pocket. S23 has larger fluctuations in hydrogen bond interactions, which may be more dynamic and can change faster. This could mean that the binding is less stable in the binding pocket. S64 shows a similar pattern to S10 but tends to be slightly more volatile at some points. This indicates moderate stability in hydrogen bond interactions. Fig. 8(c) shows that S10 is more stable in the binding pocket compared to S23, where it appears to have higher movement dynamics, while S64 has moderate stability. S10 shows relatively low and stable RMSD values throughout the simulation. This indicates that S10 tends to be stable and does not fluctuate much from its initial position in the binding pocket. S23 shows more significant RMSD fluctuations, with higher values at some time points. This indicates that S23 undergoes larger conformational changes, which may be that this molecule is not completely stable in the binding pocket. S64 shows similar RMSD values to S10, but with slightly more fluctuations. This suggests that S64 has moderate stability in the binding pocket. Fig. 8(d) shows that S10 has the most consistent conformation close to the native ligand, followed by S64 with moderate stability and S23 which is the most dynamic. S10 shows relatively low and stable RMSD values throughout

the simulation, meaning that the conformation of this molecule remains quite close to the native ligand. This stability suggests that S10 is well adapted in the binding pocket. S23 shows higher fluctuations in RMSD values, with several peaks indicating that the conformation of this molecule is more variable and less stable. These fluctuations suggest that S23 may not interact optimally in the binding pocket. S64 shows a similar pattern to S10, but with some minor fluctuations. Although stable, S64 may undergo minor changes in conformation that affect alignment with the native ligand. The low RMSD values f S10 and S64 indicate that this molecule can maintain the appropriate conformation for effective interaction with the target. Meanwhile, the higher fluctuation of S23 indicates the possible lack of affinity and effective interaction in the biological context.

Fig. 9 shows the change in binding energy during a molecular dynamics simulation time of 100 ns. Molecule S10 has a binding energy in the range of about -62 to -70 kcal/mol. The graph indicates that S10's binding energy is more constant over the simulation. Although there are minimal variations, typically the energy persists inside a limited range. The great stability of the interaction suggests that S10 has good achievable medicinal value. Stable binding energy reflects the ability of this molecule to settle at the target site. Molecule S64 has a binding energy in the range of about -58 to -65 kcal/mol. The binding energy of S64 is also relatively stable, although there are slightly more fluctuations than S10. However, overall, the energy remains within a consistent range. S64 shows a fairly strong and stable interaction, but slightly weaker than S10. Molecule S23 has a binding energy varying approximately from -58 to -62 kcal/mol. Although S23 has good stability in binding energy, its fluctuation is rather more noticeable than that of S10 and S64. This molecule shows greater instability and may be less effective in interacting with its target. The higher fluctuation of binding energy in the graph also indicates that this molecule may be more sensitive to conformational changes. S23 shows stable interaction, but its binding energy is the weakest among the three molecules. While all molecules exhibit good stability, S10 is rather more stable than S23 and S64. The strongest to weakest rank of interaction strength based on binding energy is S10 > S64 > S23. The S64 and S23 may need further modification to improve the interaction with the target.

Fig. 10 shows a comparison of the interactions between three molecules S10, S23, and S64 in each 3JSU binding pocket after molecular dynamics simulations were performed for 100 ns. Fig. 10(a) shows the presence of a hydrogen bond between S10 and Asn108 residue of 2.16 Å, interestingly there is a halogen bond with Val45 residue (3.21 Å) with one of the Cl atoms on S10, pi-silfur on Met55 residue (5.20 Å) and two stacked pi-pi bonds with Phe58. The combination of pi-stacking interactions and hydrogen bonds shows that S10 has a fairly stable interaction in the binding pocket. Fig. 10(b) shows that Met55 forms a pi-sulfur bond of 5.18 Å and Phe58 forms two stacked pi-pi bonds of 4.10 and 4.50 Å. There is one hydrogen bond with residue Val45 at 2.74, and pi-alkyl is formed with residues Ile14, Ala16, and Leu46. The stability of S23 is mainly driven by strong hydrophobic interactions. In Fig. 10(c), there are two hydrogen bonds with residues Asp54 (2.44 Å) and Phe58 (3.04 Å). Residue Val45 forms a halogen bond with the Cl atom of S64 at 3.36 Å. A stacked pi-pi bond is also formed at residue Phe58 at 4.55 Å. Meanwhile, other residues tend to form alkyl and pi -alkyl including Ile14, Ala16, Leu46, Met55, and Ile112. The combination of significant pi-stacking interactions and hydrogen bonds indicates that S64 has excellent stability in the binding pocket. In general, molecules with more interactions and stronger interactions (such as hydrogen bonding and pi-stacking) will have higher stability in the binding pocket. S10 with a combination of pi-stacking interactions and hydrophobic interactions and hydrogen bonds also shows good stability. S64 with a combination of hydrogen bonds and pi-stacking interactions, probably has the highest stability. S23 which mainly interacts through hydrophobic interactions, also shows good stability, although it may be slightly less stable than S64.

4. CONCLUSIONS

This study evaluated the chemical molecule of 4-benzyloxy-2-trichloromethylquinazoline derivatives as antiplasmodial through QSAR, ADME, drug-likeness, toxicity, molecular docking, and molecular

dynamics simulations. The best QSAR model, which demonstrated a relationship between antiplasmodial activity (pIC_{50}) and the GATS4e, SpMax_AEA(ed), Mor28e, ATS6m, and ATSC7m descriptors, was successfully developed and statistically validated by MLR and PLS. Based on this model, three new molecules S10, S23, and S64 were designed with good prediction of antiplasmodial activity, as well as showing favorable pharmacokinetic profiles and moderate to non-toxic toxicity. Molecular docking results showed higher binding energy of the new molecules with *Pf*DHFR-TS compared to the reference ligand, with the amino acid residues Leu46, Asp54, Ser111, and Thr185 playing an important role in the interaction with the receptor. Molecular dynamics simulations confirmed the stability of the interaction of the new molecule complex with *Pf*DHFR-TS for 100 ns.

LIST OF ABBREVIATIONS

*Pf*DHFR-TS	: *Plasmodium falciparum* dihydrofolate reductase–thymidylate synthase
WT *Pf*DHFR-TS	: Wild type *Pf*DHFR-TS
QM *Pf*DHFR-TS	: Quadruple mutant *Pf*DHFR-TS
3QGT	: Protein target of wild type
3JSU	: Protein target of quadruple mutant
MLR	: Multiple linear regression
PLS	: Partial least square
IC_{50}	: Half-maximal inhibitory concentration
pIC_{50}	: Potential of IC_{50}
RMSD	: Root-mean square deviation.
PRESS	: Predicted residual error sum of squares
SEE	: Standard error estimation
RMSEP	: Root-mean square error prediction
VIF	: Variance inflation factor
MF	: Mean effect
CP6	: Reference/native ligand code of wild type
QN254	: Reference/native ligand code of mutant

AUTHOR INFORMATION

Corresponding Author

Harno Dwi Pranowo — Department of Chemistry, Universitas Gadjah Mada, Yogyakarta-55281 (Indonesia); Austrian-Indonesian Centre (AIC) for Computational Chemistry, Universitas Gadjah Mada, Yogyakarta-55281 (Indonesia);

orcid.org/0000-0002-0223-5036

Email: harnodp@ugm.ac.id

Authors

Radite Yogaswara — Department of Chemistry, Universitas Gadjah Mada, Yogyakarta-55281 (Indonesia); Austrian-Indonesian Centre (AIC) for Computational Chemistry, Universitas Gadjah Mada, Yogyakarta-55281 (Indonesia); Department of Chemistry Education, Universitas Papua, Manokwari-98311 (Indonesia);

orcid.org/0000-0002-5937-6200

Niko Prasetyo — Department of Chemistry, Universitas Gadjah Mada, Yogyakarta-55281 (Indonesia); Austrian-Indonesian Centre (AIC) for Computational Chemistry, Universitas Gadjah Mada, Yogyakarta-55281 (Indonesia);

orcid.org/0000-0003-0266-7258

Maria Ludya Pulung — Department of Chemistry, Universitas Gadjah Mada, Yogyakarta-55281 (Indonesia); Department of Chemistry, Universitas Papua, Manokwari-98311 (Indonesia);

orcid.org/0000-0002-2458-7198

Author Contributions

Conceptualization, R. Y.and H. D. P.; Methodology, N. P.; Software, Resources and Visualization, M. L. P.; Supervision and Validation, H. D. P. and N. P.; Formal Analysis, Investigation, Data Curation, and Writing – Original Draft Preparation, R. Y.; Writing – Review & Editing, All authors.

Conflicts of Interest

The authors declare no conflict of interest.

SUPPORTING INFORMATION

Supplementary data associated with this article can be found in the online version at doi: 10.47352/jmans.2774-3047.258

ACKNOWLEDGEMENT

The authors express their gratitude to the Final Project Recognition Grant (RTA) of Universitas Gadjah Mada (5286/UN1.P1/PT.01.03/2024) and the first author thanks the Indonesian Endowment Fund for Education (LPDP), the Ministry of Finance, and the Republic of Indonesia for the scholarship received to pursue their doctoral studies at Gadjah Mada University (2022–2026). The authors acknowledge the Cresset Discovery Group for providing Spark free licenses.

REFERENCES

[1] M. Fikadu and E. Ashenafi. (2023). "Malaria: An Overview". *Infection and Drug Resistance.* **16** : 3339-3347. 10.2147/IDR.S405668.

[2] F. M. Wunsch, B. Wunsch, F. A. Bernal, and T. J. Schmidt. (2021). "Quantitative Structure -Activity Relationships of Natural-Product-Inspired, Aminoalkyl-Substituted 1-Benzopyrans as Novel Antiplasmodial Agents". *Molecules.* **26** (17). 10.3390/molecules26175249.

[3] S. Rout and R. K. Mahapatra. (2019). "Plasmodium falciparum: Multidrug resistance". *Chemical Biology & Drug Design.* **93** (5): 737-759. 10.1111/cbdd.13484.

[4] A. K. Pandey, V. Baboo, V. N. Mishra, V. K. Singh, and A. Dwivedi. (2020). "Comparative Study of Molecular Docking, Structural, Electronic, Vibrational Spectra and Fukui Function Studies of Thiadiazole Containing Schiff Base – A Complete Density Functional Study". *Polycyclic Aromatic Molecules.* **42** (1): 13-39. 10.1080/10406638.2020.1712440.

[5] J. Yuvaniyama, P. Chitnumsub, S. Kamchonwongpaisan, J. Vanichtanankul, W. Sirawaraporn, P. Taylor, M. D. Walkinshaw, and Y. Yuthavong. (2003). "Insights into antifolate resistance from malarial DHFR-TS structures". *Nature Structural & Molecular Biology.* **10** (5): 357-65. 10.1038/nsb921.

[6] A. Nzila, M. Rottmann, P. Chitnumsub, S. M. Kiara, S. Kamchonwongpaisan, C. Maneeruttanarungroj, S. Taweechai, B. K. Yeung, A. Goh, S. B. Lakshminarayana, B. Zou, J. Wong, N. L. Ma, M. Weaver, T. H. Keller, V. Dartois, S. Wittlin, R. Brun, Y. Yuthavong, and T. T. Diagana. (2010). "Preclinical evaluation of the antifolate QN254, 5-chloro- N'6'-(2,5-dimethoxy-benzyl)-quinazoline-2,4,6-triamine, as an antimalarial drug candidate". *Antimicrobial Agents and Chemotherapy.* **54** (6): 2603-10. 10.1128/AAC.01526-09.

[7] C. Roper, R. Pearce, B. Bredenkamp, J. Gumede, C. Drakeley, F. Mosha, D. Chandramohan, and B. Sharp. (2003). "Antifolate antimalarial resistance in southeast Africa: a population-based analysis". *Lancet.* **361** (9364): 1174-81. 10.1016/S0140-6736(03)12951-0.

[8] Y. Yuthavong, J. Yuvaniyama, P. Chitnumsub, J. Vanichtanankul, S. Chusacultanachai, B. Tarnchompoo, T. Vilaivan, and S. Kamchonwongpaisan. (2005). "Malarial (Plasmodium falciparum) dihydrofolate reductase-thymidylate synthase: structural basis for antifolate resistance and development of effective inhibitors". *Parasitology.* **130** (Pt 3): 249-59. 10.1017/s003118200400664x.

[9] E. Kenangalem, J. R. Poespoprodjo, N. M. Douglas, F. H. Burdam, K. Gdeumana, F. Chalfein, Prayoga, F. Thio, A. Devine, J. Marfurt, G. Waramori, S. Yeung, R. Noviyanti, P. Penttinen, M. J. Bangs, P. Sugiarto, J. A. Simpson, Y. Soenarto, N. M. Anstey, and R. N. Price. (2019). "Malaria morbidity and mortality following introduction of a universal policy of artemisinin-based treatment for malaria in Papua, Indonesia: A longitudinal surveillance study". *PLOS Medicine.* **16** (5): e1002815. 10.1371/journal.pmed.1002815.

[10] H. R. Bhat, P. K. Pandey, S. K. Ghosh, and U. P. Singh. (2013). "Development of 4-

aminoquinoline-1,3,5-triazine conjugates as potent antibacterial agent through facile synthetic route". *Medicinal Chemistry Research.* **22** (10): 5056-5065. 10.1007/s00044-013-0521-8.

[11] S. Balabadra, M. Kotni, V. Manga, A. D. Allanki, R. Prasad, and P. S. Sijwali. (2017). "Synthesis and evaluation of naphthyl bearing 1,2,3-triazole analogs as antiplasmodial agents, cytotoxicity and docking studies". *Bioorganic & Medicinal Chemistry.* **25** (1): 221-232. 10.1016/j.bmc.2016.10.029.

[12] M. Aarjane, S. Slassi, and A. Amine. (2021). "Synthesis, antibacterial evaluation and computational studies of new acridone-1,2,3-triazole hybrids". *Journal of Molecular Structure.* **1241**. 10.1016/j.molstruc.2021.130636.

[13] R. A. Azzam, R. E. Elsayed, and G. H. Elgemeie. (2020). "Design, Synthesis, and Antimicrobial Evaluation of a New Series of N-Sulfonamide 2-Pyridones as Dual Inhibitors of DHPS and DHFR Enzymes". *ACS Omega.* **5** (18): 10401-10414. 10.1021/acsomega.0c00280.

[14] S. Shahzad, M. A. Qadir, M. Ahmed, S. Ahmad, M. J. Khan, A. Gulzar, and M. Muddassar. (2020). "Folic acid-sulfonamide conjugates as antibacterial agents: design, synthesis and molecular docking studies". *RSC Advances.* **10** (70): 42983-42992. 10.1039/d0ra09051d.

[15] D. J. Christian, R. H. Vekariya, K. D. Patel, D. P. Rajani, S. D. Rajani, K. Parmar, M. T. Chhabaria, and H. D. Patel. (2020). "Molecular Docking and QSAR Study of Chalcone and Pyrimidine Derivatives as Potent Anti-Malarial Agents against Plasmodium falciparum". *International Letters of Chemistry, Physics and Astronomy.* **85** : 23-34. 10.56431/p-75shdg.

[16] J. Syahri, H. Nasution, B. A. Nurohmah, B. Purwono, E. Yuanita, N. H. Zakaria, and N. I. Hassan. (2020). "Design, Synthesis and Biological Evaluation of Aminoalkylated Chalcones as Antimalarial Agent". *Sains Malaysiana.* **49** (11): 2667-2677. 10.17576/jsm-2020-4911-06.

[17] J. Syahri, E. Yuanita, B. Achromi Nurohmah, M. Hizbul Wathon, R. Syafri, R. Armunanto, and B. Purwono. (2017). "Xanthone as Antimalarial: QSAR Analysis, Synthesis, Molecular Docking and In-vitro Antimalarial Evaluation". *Oriental Journal of Chemistry.* **33** (1): 29-40. 10.13005/ojc/330104.

[18] A. Gellis, N. Primas, S. Hutter, G. Lanzada, V. Remusat, P. Verhaeghe, P. Vanelle, and N. Azas. (2016). "Looking for new antiplasmodial quinazolines: DMAP-catalyzed synthesis of 4-benzyloxy- and 4-aryloxy-2-trichloromethylquinazolines and their in vitro evaluation toward Plasmodium falciparum". *European Journal of Medicinal Chemistry.* **119** : 34-44. 10.1016/j.ejmech.2016.04.059.

[19] R. Karan, P. Agarwal, M. Sinha, and N. Mahato. (2021). "Recent Advances on Quinazoline Derivatives: A Potential Bioactive Scaffold in Medicinal Chemistry". *ChemEngineering.* **5** (4). 10.3390/chemengineering5040073.

[20] A. Dutta and D. Sarma. (2020). "Recent advances in the synthesis of Quinazoline analogues as Anti-TB agents". *Tuberculosis (Edinb).* **124** : 101986. 10.1016/j.tube.2020.101986.

[21] C. Castera-Ducros, N. Azas, P. Verhaeghe, S. Hutter, P. Garrigue, A. Dumetre, L. Mbatchi, M. Laget, V. Remusat, F. Sifredi, S. Rault, P. Rathelot, and P. Vanelle. (2011). "Targeting the human malaria parasite Plasmodium falciparum: in vitro identification of a new antiplasmodial hit in 4-phenoxy-2-trichloromethylquinazoline series". *European Journal of Medicinal Chemistry.* **46** (9): 4184-91. 10.1016/j.ejmech.2011.06.021.

[22] P. Verhaeghe, A. Dumetre, C. Castera-Ducros, S. Hutter, M. Laget, C. Fersing, M. Prieri, J. Yzombard, F. Sifredi, S. Rault, P. Rathelot, P. Vanelle, and N. Azas. (2011). "4-Thiophenoxy-2-trichloromethyquinazolines display in vitro selective antiplasmodial activity against the human malaria parasite Plasmodium falciparum". *Bioorganic & Medicinal Chemistry Letters.* **21** (19): 6003-6. 10.1016/j.bmcl.2011.06.113.

[23] P. S. Auti, G. George, and A. T. Paul. (2020). "Recent advances in the pharmacological diversification of quinazoline/quinazolinone hybrids". *RSC Advances.* **10** (68): 41353-41392. 10.1039/d0ra06642g.

[24] V. Alagarsamy, K. Chitra, G. Saravanan, V. R. Solomon, M. T. Sulthana, and B. Narendhar. (2018). "An overview of quinazolines: Pharmacological significance and recent developments". *European Journal of Medicinal Chemistry.* **151** : 628-685. 10.1016/j.ejmech.2018.03.076.

[25] M. Saeedi, M. Mohammadi-Khanaposhtani, P. Pourrabia, N. Razzaghi, R. Ghadimi, S. Imanparast, M. A. Faramarzi, F. Bandarian, E. N. Esfahani, M. Safavi, H. Rastegar, B. Larijani, M. Mahdavi, and T. Akbarzadeh. (2019). "Design and synthesis of novel quinazolinone-1,2,3-triazole hybrids as new anti-diabetic agents: In vitro alpha-glucosidase inhibition, kinetic, and docking study". *Bioorganic Chemistry.* **83** : 161-169. 10.1016/j.bioorg.2018.10.023.

[26] T. S. Patel, J. D. Bhatt, R. B. Dixit, C. J. Chudasama, B. D. Patel, and B. C. Dixit. (2019). "Green synthesis, biological evaluation, molecular docking studies and 3D -QSAR analysis of novel phenylalanine linked quinazoline-4(3H)-one-sulphonamide hybrid entities distorting the malarial reductase activity in folate pathway". *Bioorganic & Medicinal Chemistry.* **27** (16): 3574-3586. 10.1016/j.bmc.2019.06.038.

[27] P. Pathak, V. Naumovich, M. Grishina, P. K. Shukla, A. Verma, and V. Potemkin. (2019). "Quinazoline based 1,3,5-triazine derivatives as cancer inhibitors by impeding the phosphorylated RET tyrosine kinase pathway: Design, synthesis, docking, and QSAR study". *Archiv der Pharmazie.* **352** (9): e1900053. 10.1002/ardp.201900053.

[28] O. O. Ajani, D. V. Aderohunmu, E. N. Umeokoro, and A. O. Olomieja. (2016). "Quinazoline pharmacophore in therapeutic medicine". *Bangladesh Journal of Pharmacology.* **11** (3). 10.3329/bjp.v11i3.25731.

[29] R. S. Cheke, S. D. Shinde, J. P. Ambhore, S. R. Chaudhari, and S. B. Bari. (2022). "Quinazoline: An update on current status against convulsions". *Journal of Molecular Structure.* **1248**. 10.1016/j.molstruc.2021.131384.

[30] P. Jiwamurwa Pama Tjitda, F. O. Nitbani, and D. Mbunga. (2022). "QSAR and Molecular Docking of Pyrimidine Derivatives Against Plasmodium falciparum dihydrofolate reductase-thymidylate synthase (PfDHFR-TS)". *Journal of Research in Pharmacy.* **26(6)** (26(6)): 1723-1735. 10.29228/jrp.284.

[31] Y. S. Kurniawan, T. Indriani, H. Amrulloh, L. C. Adi, A. C. Imawan, K. T. A. Priyangga, and E. Yudha. (2023). "The Journey of Natural Products: From Isolation Stage to Drug's Approval in Clinical Trials". *Bioactivities.* **1** (2): 43-60. 10.47352/bioactivities.2963-654X.190.

[32] I. Arief, H. D. Pranowo, M. Mudasir, and K. Wijaya. (2021). "QSAR-Based Design of Potent Betulinic Acid Derivatives as HIV Maturation Inhibitors". *Chiang Mai University Journal of Natural Sciences.* **20** (1): e2021010.

[33] A. W. Mahmud, G. A. Shallangwa, and A. Uzairu. (2020). "QSAR and molecular docking studies of 1,3-dioxoisoindoline-4-aminoquinolines as potent antiplasmodium hybrid molecules". *Heliyon.* **6** (3): e03449. 10.1016/j.heliyon.2020.e03449.

[34] F. D. Prieto-Martínez, E. López-López, K. Eurídice Juárez-Mercado, and J. L. Medina-Franco. (2019). In: "In Silico Drug Design". 19-44. 10.1016/b978-0-12-816125-8.00002-x.

[35] A. Das, M. Sarangi, K. Jangid, V. Kumar, A. Kumar, P. P. Singh, K. Kaur, V. Kumar, S. Chakraborty, and V. Jaitak. (2024). "Identification of 1,3,4-oxadiazoles as tubulin -targeted anticancer agents: a combined field-based 3D-QSAR, pharmacophore model-based virtual screening, molecular docking, molecular dynamics simulation, and density functional theory calculation approach". *Journal of Biomolecular Structure and Dynamics.* **42** (19): 10323-10341. 10.1080/07391102.2023.2256876.

[36] M. Er-Rajy, M. El Fadili, N. N. Mrabti, S.

Zarougui, and M. Elhallaoui. (2022). "QSAR, molecular docking, ADMET properties in silico studies for a series of 7-propanamide benzoxaboroles as potent anti-cancer agents". *Chinese Journal of Analytical Chemistry.* **50** (12). 10.1016/j.cjac.2022.100163.

[37] S. Moshawih, H. P. Goh, N. Kifli, M. A. E. Darwesh, C. Ardianto, K. W. Goh, and L. C. Ming. (2024). "Identification and optimization of TDP1 inhibitors from anthraquinone and chalcone derivatives: consensus scoring virtual screening and molecular simulations". *Journal of Biomolecular Structure and Dynamics.* **42** (19): 10286-10310. 10.1080/07391102.2023.2256870.

[38] P. M. Khan and K. Roy. (2018). "Current approaches for choosing feature selection and learning algorithms in quantitative structure-activity relationships (QSAR)". *Expert Opinion on Drug Discovery.* **13** (12): 1075-1089. 10.1080/17460441.2018.1542428.

[39] A. Tropsha. (2010). "Best Practices for QSAR Model Development, Validation, and Exploitation". *Molecular Informatics.* **29** (6-7): 476-88. 10.1002/minf.201000061.

[40] A. Mauri. (2020). In: "Ecotoxicological QSARs, (Methods in Pharmacology and Toxicology, ch. Chapter 32". 801-820. 10.1007/978-1-0716-0150-1_32.

[41] Z. Y. u. Ibrahim, A. Uzairu, G. Shallangwa, and S. Abechi. (2020). "QSAR and molecular docking based design of some indolyl-3-ethanone-α-thioethers derivatives as Plasmodium falciparum dihydroorotate dehydrogenase (PfDHODH) inhibitors". *SN Applied Sciences.* **2** (7). 10.1007/s42452-020-2955-1.

[42] M. Abdullahi, A. Uzairu, G. A. Shallangwa, P. A. Mamza, and M. T. Ibrahim. (2022). "2D-QSAR, 3D-QSAR, molecular docking and ADMET prediction studies of some novel 2-((1H-indol-3-yl)thio)-N-phenyl-acetamide derivatives as anti-influenza A virus". *Egyptian Journal of Basic and Applied Sciences.* **9** (1): 510-532. 10.1080/2314808x.2022.2108592.

[43] Y. E. Masaoudy, I. Aanouz, Y. Moukhliss, Y. Koubi, H. Maghat, T. Lakhlifi, and M. Bouachrine. (2020). "2D-QSAR study of the antimicrobial activity of a series of 5-(substituted benzaldehyde) thiazolidine-2,4-dione derivatives against Staphylococcus aureus by Multiple Linear Regression method". *Journal of Materials and Environmental Science.* **11** (11): 1914-1927.

[44] K. Tabti, A. Sbai, H. Maghat, M. Bouachrine, and T. Lakhlifi. (2020). "2D and 3D-QSAR/ CoMSIA Comparative Study On a Series of Thiazole Derivatives as SDHI Inhibitors". *Maghrebian Journal of Pure and Applied Science.* **6** (2): 73-90.

[45] B. Raju, B. Sapra, and O. Silakari. (2023). "3D-QSAR assisted identification of selective CYP1B1 inhibitors: an effective bioisosteric replacement/molecular docking/ electrostatic complementarity analysis". *Molecular Diversity.* **27** (6): 2673-2693. 10.1007/s11030-022-10574-7.

[46] A. Dick and S. Cocklin. (2020). "Bioisosteric Replacement as a Tool in Anti-HIV Drug Design". *Pharmaceuticals (Basel).* **13** (3). 10.3390/ph13030036.

[47] J. B. Ghasemi and F. Shiri. (2011). "Molecular docking and 3D-QSAR studies of falcipain inhibitors using CoMFA, CoMSIA, and Open3DQSAR". *Medicinal Chemistry Research.* **21** (10): 2788-2806. 10.1007/s00044-011-9803-1.

[48] T. I. Netzeva, A. Worth, T. Aldenberg, R. Benigni, M. T. Cronin, P. Gramatica, J. S. Jaworska, S. Kahn, G. Klopman, C. A. Marchant, G. Myatt, N. Nikolova-Jeliazkova, G. Y. Patlewicz, R. Perkins, D. Roberts, T. Schultz, D. W. Stanton, J. J. van de Sandt, W. Tong, G. Veith, and C. Yang. (2005). "Current status of methods for defining the applicability domain of (quantitative) structure-activity relationships. The report and recommendations of ECVAM Workshop 52". *Alternatives to Laboratory Animals.* **33** (2): 155-73. 10.1177/026119290503300209.

[49] P. Gramatica. (2007). "Principles of QSAR models validation: internal and external". *QSAR & Combinatorial Science.* **26** (5): 694-701. 10.1002/qsar.200610151.

[50] W. P. Walters. (2012). "Going further than Lipinski's rule in drug design". *Expert*

Opinion on Drug Discovery. **7** (2): 99-107. 10.1517/17460441.2012.648612.

[51] A. K. Ghose, V. N. Viswanadhan, and J. J. Wendoloski. (1999). "A knowledge-based approach in designing combinatorial or medicinal chemistry libraries for drug discovery. 1. A qualitative and quantitative characterization of known drug databases". *Journal of Combinatorial Chemistry.* **1** (1): 55-68. 10.1021/cc9800071.

[52] D. F. Veber, S. R. Johnson, H. Y. Cheng, B. R. Smith, K. W. Ward, and K. D. Kopple. (2002). "Molecular properties that influence the oral bioavailability of drug candidates". *Journal of Medicinal Chemistry.* **45** (12): 2615-23. 10.1021/jm020017n.

[53] W. J. Egan, K. M. Merz, Jr., and J. J. Baldwin. (2000). "Prediction of drug absorption using multivariate statistics". *Journal of Medicinal Chemistry.* **43** (21): 3867-77. 10.1021/jm000292e.

[54] I. Muegge, S. L. Heald, and D. Brittelli. (2001). "Simple selection criteria for drug-like chemical matter". *Journal of Medicinal Chemistry.* **44** (12): 1841-6. 10.1021/jm015507e.

[55] Y. C. Martin. (2005). "A bioavailability score". *Journal of Medicinal Chemistry.* **48** (9): 3164-70. 10.1021/jm0492002.

[56] A. Daina, O. Michielin, and V. Zoete. (2017). "SwissADME: a free web tool to evaluate pharmacokinetics, drug-likeness and medicinal chemistry friendliness of small molecules". *Scientific Reports.* **7** : 42717. 10.1038/srep42717.

[57] C. Hansch, A. Leo, S. B. Mekapati, and A. Kurup. (2004). "QSAR and ADME". *Bioorganic & Medicinal Chemistry.* **12** (12): 3391-400. 10.1016/j.bmc.2003.11.037.

[58] Z. Jin, Y. Wang, X. F. Yu, Q. Q. Tan, S. S. Liang, T. Li, H. Zhang, P. C. Shaw, J. Wang, and C. Hu. (2020). "Structure-based virtual screening of influenza virus RNA polymerase inhibitors from natural molecules: Molecular dynamics simulation and MM-GBSA calculation". *Computational Biology and Chemistry.* **85** : 107241. 10.1016/j.compbiolchem.2020.107241.

[59] S. Chtita, A. Aouidate, A. Belhassan, A. Ousaa, A. I. Taourati, B. Elidrissi, M. Ghamali, M. Bouachrine, and T. Lakhlifi. (2020). "QSAR study of N-substituted oseltamivir derivatives as potent avian influenza virus H5N1 inhibitors using quantum chemical descriptors and statistical methods". *New Journal of Chemistry.* **44** (5): 1747-1760. 10.1039/c9nj04909f.

[60] F. Cheng, W. Li, Y. Zhou, J. Shen, Z. Wu, G. Liu, P. W. Lee, and Y. Tang. (2012). "admetSAR: a comprehensive source and free tool for assessment of chemical ADMET properties". *Journal of Chemical Information and Modeling.* **52** (11): 3099-105. 10.1021/ci300367a.

[61] L. Guan, H. Yang, Y. Cai, L. Sun, P. Di, W. Li, G. Liu, and Y. Tang. (2019). "ADMET-score - a comprehensive scoring function for evaluation of chemical drug-likeness". *Medchemcomm.* **10** (1): 148-157. 10.1039/c8md00472b.

[62] A. M. Viana Nunes, F. das Chagas Pereira de Andrade, L. A. Filgueiras, O. A. de Carvalho Maia, R. Cunha, S. V. A. Rodezno, A. L. M. Maia Filho, F. A. de Amorim Carvalho, D. C. Braz, and A. N. Mendes. (2020). "preADMET analysis and clinical aspects of dogs treated with the Organotellurium molecule RF07: A possible control for canine visceral leishmaniasis?". *Environmental Toxicology and Pharmacology.* **80** : 103470. 10.1016/j.etap.2020.103470.

[63] L. Fu, S. Shi, J. Yi, N. Wang, Y. He, Z. Wu, J. Peng, Y. Deng, W. Wang, C. Wu, A. Lyu, X. Zeng, W. Zhao, T. Hou, and D. Cao. (2024). "ADMETlab 3.0: an updated comprehensive online ADMET prediction platform enhanced with broader coverage, improved performance, API functionality and decision support". *Nucleic Acids Research.* **52** (W1): W422-W431. 10.1093/nar/gkae236.

[64] D. E. Pires, T. L. Blundell, and D. B. Ascher. (2015). "pkCSM: Predicting Small-Molecule Pharmacokinetic and Toxicity Properties Using Graph-Based Signatures". *Journal of Medicinal Chemistry.* **58** (9): 4066-72. 10.1021/acs.jmedchem.5b00104.

[65] P. Banerjee, E. Kemmler, M. Dunkel, and R. Preissner. (2024). "ProTox 3.0: a webserver

for the prediction of toxicity of chemicals". *Nucleic Acids Research.* **52** (W1): W513-W520. 10.1093/nar/gkae303.

[66] Y. Yeni and R. A. Rachmania. (2023). "Toxicity of Anti-Inflammatory Substances in Hemigraphis Alternata Leaves: In Silico Study Using ProTox-II". *Jurnal Sains dan Kesehatan.* **5** (5): 810-815. 10.25026/jsk.v5i5.1975.

[67] R. Yogaswara, M. L. Pulung, S. H. Yuliani, and E. P. Istyastono. (2020). "Docking-Guided 3D-QSAR Studies of 4-Aminoquinoline-1,3,5-triazines as Inhibitors for Plasmodium falciparum Dihydrofolate Reductase". *Indonesian Journal of Chemistry.* **20** (6). 10.22146/ijc.50674.

[68] G. Nugraha and E. P. Istyastono. (2021). "Virtual Target Construction for Structure-Based Screening in the Discovery of Histamine H2 Receptor Ligands". *International Journal of Applied Pharmaceutics.* 239-241. 10.22159/ijap.2021v13i3.41202.

[69] T. Steinbrecher and A. Labahn. (2010). "Towards accurate free energy calculations in ligand protein-binding studies". *Current Medicinal Chemistry.* **17** (8): 767-85. 10.2174/092986710790514453.

[70] V. Limongelli. (2020). "Ligand binding free energy and kinetics calculation in 2020". *WIREs Computational Molecular Science.* **10** (4). 10.1002/wcms.1455.

[71] Y. S. Kurniawan, E. Yudha, G. Nugraha, N. Fatmasari, H. D. Pranowo, J. Jumina, and E. N. Sholikhah. (2024). "Molecular Docking and Molecular Dynamic Investigations of Xanthone-Chalcone Derivatives against Epidermal Growth Factor Receptor for Preliminary Discovery of Novel Anticancer Agent". *Indonesian Journal of Chemistry.* **24** (1). 10.22146/ijc.88449.

[72] M. El Faydy, L. Lakhrissi, N. Dahaieh, K. Ounine, B. Tuzun, N. Chahboun, A. Boshaala, A. AlObaid, I. Warad, B. Lakhrissi, and A. Zarrouk. (2024). "Synthesis, Biological Properties, and Molecular Docking Study of Novel 1,2,3-Triazole-8-quinolinol Hybrids". *ACS Omega.* **9** (23): 25395-25409. 10.1021/acsomega.4c03906.

[73] T. Venianakis, C. Oikonomaki, M. G. Siskos, A. Primikyri, and I. P. Gerothanassis. (2021). "DFT Calculations of (1)H NMR Chemical Shifts of Geometric Isomers of Conjugated Linolenic Acids, Hexadecatrienyl Pheromones, and Model Triene-Containing Molecules: Structures in Solution and Revision of NMR Assignments". *Molecules.* **26** (11). 10.3390/molecules26113477.

[74] V. A. Semenov and L. B. Krivdin. (2020). "DFT computational schemes for (1) H and (13) C NMR chemical shifts of natural products, exemplified by strychnine". *Magnetic Resonance in Chemistry.* **58** (1): 56-64. 10.1002/mrc.4922.

[75] N. Grimblat and A. M. Sarotti. (2016). "Computational Chemistry to the Rescue: Modern Toolboxes for the Assignment of Complex Molecules by GIAO NMR Calculations". *Chemistry.* **22** (35): 12246-61. 10.1002/chem.201601150.

[76] P. Gao, J. Zhang, Q. Peng, J. Zhang, and V. A. Glezakou. (2020). "General Protocol for the Accurate Prediction of Molecular (13)C/(1)H NMR Chemical Shifts via Machine Learning Augmented DFT". *Journal of Chemical Information and Modeling.* **60** (8): 3746-3754. 10.1021/acs.jcim.0c00388.

[77] G. Sliwoski, J. Mendenhall, and J. Meiler. (2016). "Autocorrelation descriptor improvements for QSAR: 2DA_Sign and 3DA_Sign". *Journal of Computer-Aided Molecular Design.* **30** (3): 209-17. 10.1007/s10822-015-9893-9.

[78] A. Mauri and M. Bertola. (2022). "Alvascience: A New Software Suite for the QSAR Workflow Applied to the Blood-Brain Barrier Permeability". *International Journal of Molecular Sciences.* **23** (21). 10.3390/ijms232112882.

[79] J. Afsar, S. Brij Kishore, and S. Vishnu Dutt. (2021). "Quantitative structure-activity relationship study on the MMP-13 inhibitory activity of fused pyrimidine derivatives possessing a 1,2,4-Triazol-3-yl group as a ZBG". *GSC Biological and Pharmaceutical Sciences.* **16** (1): 251-265. 10.30574/

gscbps.2021.16.1.0199.

[80] J. Yuan, S. Yu, S. Gao, Y. Gan, Y. Zhang, T. Zhang, Y. Wang, L. Yang, J. Shi, and W. Yao. (2016). "Predicting the biological activities of triazole derivatives as SGLT2 inhibitors using multilayer perceptron neural network, support vector machine, and projection pursuit regression models". *Chemometrics and Intelligent Laboratory Systems.* **156** : 166-173. 10.1016/j.chemolab.2016.06.002.

[81] Z. Amini, M. H. Fatemi, and S. Gharaghani. (2016). "Hybrid docking-QSAR studies of DPP-IV inhibition activities of a series of aminomethyl-piperidones". *Computational Biology and Chemistry.* **64** : 335-345. 10.1016/j.compbiolchem.2016.08.003.

[82] Z. Ya'u Ibrahim, A. Uzairu, G. A. Shallangwa, S. E. Abechi, and S. Isyaku. (2022). "Quantitative Structure-Activity Relationship, Structure-based Design, and ADMET studies of pyrimethamine and cycloguanil analogs inhibitors of Plasmodium falciparum dihydrofolate reductase-thymidylate synthase (PfDHFR-TS)". *Chemical Physics Impact.* **5**. 10.1016/j.chphi.2022.100132.

[83] K. S. Kannan and K. Manoj. (2015). "Outlier detection in multivariate data". *Applied Mathematical Sciences.* **9** : 2317-2324. 10.12988/ams.2015.53213.

[84] C. P. Dhakal. (2017). "Dealing with Outliers and Influential Points While Fitting Regression". *Journal of Institute of Science and Technology.* **22** (1): 61-65. 10.3126/jist.v22i1.17741.

[85] G. Tedesco.). "Using the Spark reagent databases to identify bioisosteric R-group replacements". 1-7.

[86] Y. Yuthavong, B. Tarnchompoo, T. Vilaivan, P. Chitnumsub, S. Kamchonwongpaisan, S. A. Charman, D. N. McLennan, K. L. White, L. Vivas, E. Bongard, C. Thongphanchang, S. Taweechai, J. Vanichtanankul, R. Rattanajak, U. Arwon, P. Fantauzzi, J. Yuvaniyama, W. N. Charman, and D. Matthews. (2012). "Malarial dihydrofolate reductase as a paradigm for drug development against a resistance-compromised target". *Proceedings of the National Academy of Sciences.* **109** (42): 16823-8. 10.1073/pnas.1204556109.